Evidence for large disturbances of the Ediacaran geomagnetic field from West Africa

Boris Robert [a b 1*], Fernando Corfu [a], Mathew Domeier [a d], Olivier Blein [c]

[a] Centre for Earth Evolution and Dynamics (CEED), University of Oslo, Norway

[b] Geodynamic Modelling Section, GeoForschungZentrum (GFZ), Germany

[c] Bureau de Recherches Géologiques et Minières (BRGM), Orléans, France

[d] Centre for Planetary Habitability (PHAB), University of Oslo, Norway

[1] now at Institut de Physique du Globe de Paris, Université Paris Cité, France

* corresponding author: brobert@ipgp.fr

This manuscript has been peer-reviewed and published in *Precambrian Research*, DOI: https://doi.org/10.1016/j.precamres.2023.107095

Evidence for large disturbances of the Ediacaran Geomagnetic field from West Africa

Boris Robert[1,2,*], Fernando Corfu[1], Mathew Domeier[1], Olivier Blein[3]

[1] Centre for Earth Evolution and Dynamics, University of Oslo, Norway

[2] Geodynamic Modelling Section, GFZ, Germany

[3] BRGM, Orléans, France

[*] now at Institut de Physique du Globe de Paris, Université Paris Cité, France

Keywords: True Polar Wander, Paleomagnetism, Ediacaran, Magnetic Field, Precambrian

Abstract

Constraining the paleogeography of the Ediacaran is crucial for understanding the extensive tectonic, biological and geochemical changes that occurred during that epoch. Paleomagnetism is an essential tool for reconstructing the Ediacaran paleogeography but it is complicated because the paleomagnetic data of that age display unusually fast and large directional oscillations. Two main competing hypotheses have been proposed: the occurrence of very fast True Polar Wander (TPW) episodes, which correspond to the motion of the planetary spin axis relative to the solid Earth, or strong geomagnetic field disturbances that could potentially be dominated by an equatorial dipole field. Their implications for paleogeographic reconstructions are radically different as TPW would result in a major latitudinal shift of continents of up to ~90°. In this study, we focus on one rapid paleomagnetic change recorded in pyroclastic rocks of the Ouarzazate Group in the Anti-Atlas Belt (Morocco) that has been interpreted to reflect an exceptionally fast episode of True Polar Wander between ~575 and 565 Ma. To further test this hypothesis, tight constraints on the rate of the paleomagnetic directional change are needed, as TPW is speed-limited by mantle viscosity. Here, we present high-resolution Chemical Abrasion Isotope-Dilution Thermal Ionization Mass Spectrometry (CA-ID-TIMS) U-Pb dates on zircons from seven pyroclastic levels distributed stratigraphically below, in between and above the horizons where the large paleomagnetic change is observed. Based on these new data, we estimate the associated lower bound rate of the polar motion related to this abrupt paleomagnetic change to be 11.6°/Myrs [5.5 – 17.9]. This value is much higher than the TPW speed limit estimated from numerical simulations, suggesting that this large paleomagnetic change cannot be explained by TPW. It could rather be associated with intense perturbations of the Ediacaran geomagnetic field potentially oscillating from an axial to an equatorial dipole. The paleomagnetic pole that we interpret as referring to the axial dipole field would imply that West Africa was located at high latitude during the mid-Ediacaran.

1. Introduction

The Ediacaran (635-539 Ma) is a fascinating period of the Earth's history marked by considerable changes in the superficial layers of the planet including rapid biological evolution, large disruptions in the carbon cycle and the occurrence of glaciations on many continents (e.g. Xiao and Narbonne, 2020). Paleogeography, a major forcing in the evolution of the Earth's surface, also changed dramatically during this period with the final breakup of the supercontinent Rodinia and the amalgamation of Gondwana (e.g. Li et al. 2008). However, quantitative Ediacaran paleogeographic models are still very controversial because paleomagnetic data remain sparse but also very scattered, rendering their interpretation challenging. The paleomagnetic record displays exceptionally fast directional changes from many continents that imply abrupt and large swings in their respective apparent polar wander paths (APWP). Several hypotheses have been proposed to explain these data (see Domeier et al., 2023 for a review): (1) ultra-high plate motion, (2) the presence of remagnetization (Hodych et al., 2004; Bono and Tarduno, 2015), (3) perturbation of the Earth's magnetic field (Abrajevitch and van der Voo, 2010; Halls et al., 2015) potentially linked to the crystallization of the inner-core (Bono et al., 2019) and (4) rapid True Polar Wander (TPW) (Kirschvink et al. 1997; Evans, 1998). The latter mechanism corresponds to the coherent motion of the solid Earth relative to the spin axis resulting from changes in the internal distribution of mass heterogeneities. While validation of hypothesis (2) would raise questions about our ability to identify remagnetizations in deep-time, hypotheses (1), (3) and (4) would have dramatic implications for our understanding of mantle and/or core processes during the Ediacaran.

In this study, we focus on the large and rapid paleomagnetic swath recorded in the APWP of West Africa around 575-565 Ma (Fig. 1; Robert et al., 2017). This segment, 111.2 ± 31.3° long, relies on two paleomagnetic poles obtained in the Ouarzazate Group, a succession of pyroclastic rocks that outcrops in the Anti-Atlas belt of Morocco. The two poles (called 'B1' and 'C' by Robert et al. 2017) are both supported by paleomagnetic field tests. Pole B1 is supported by a positive fold test, constraining the age of magnetization to predate the Hercynian orogeny (~320-260 Ma), and by a positive intraformational conglomerate test that suggests that the magnetization is primary. Pole C is supported by a positive fold test performed in an Ediacaran-age fold, suggesting that the age of magnetization is syn-Ediacaran. These two poles have therefore been interpreted as primary. This track of the West Africa APWP has been spatially and temporally correlated with similarly large and abrupt swings in the APWPs of Laurentia, Baltica, Australia and Avalonia (Robert et al., 2017, 2018; Wen et al., 2020, 2022), suggesting that this large paleomagnetic change is global and could be produced by TPW. By combining paleogeography and mantle dynamic modelling, Robert et al. (2018) found that a large reorganization of the mantle flow at the beginning of the Ediacaran could produce an extremely large displacement of the rotation axis relative to the Earth's surface. Such a dramatic episode of TPW would imply a motion of the magnetic pole with a rate and amplitude comparable to the paleomagnetic observations. However, even in such an extreme scenario, the speed of TPW is rate-limited to a few degrees per Myrs by the mantle's viscosity, which controls how fast the mantle deforms and thus the rate at which mass heterogeneities can move.

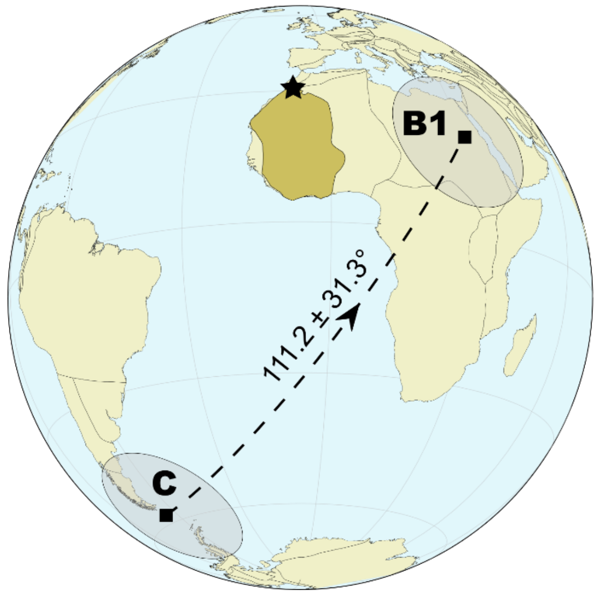

Figure 1: *Large polar shift recorded in the apparent polar wander path of West Africa around 575-565 Ma. Poles B1 and C are from the study of Robert et al. (2017). The respective sampling sites are located in the northern tip of West Africa (black star).*

Because TPW is speed-limited by mantle viscosity, the rate of change of apparent polar wander is an important parameter to assess the hypothesis of TPW, as noted by several authors (Steinberger and O'Connel, 2002; Tsai and Stevenson, 2007). Critical to this assessment of speed are the geochronological constraints associated with each paleomagnetic pole. The poles B1 and C have been dated by the Sensitive High Resolution Ion Microprobe (SHRIMP) U-Pb method on zircons, yielding age uncertainties of about 1% of their respective mean age. These age constraints allow for rates of change ranging from a few degrees per Myrs, compatible with TPW, to rates much higher than 10 degrees per Myrs, which are incompatible with TPW but could instead be explained by perturbations of the Earth's magnetic field (Abrajevitch and van der Voo, 2010). The available geochronological data are therefore not precise enough to test the hypothesis of TPW around 575-565 Ma. In this study, we provide new high-precision CA-ID-TIMS (Chemical Abrasion Isotope-Dilution Thermal Ionization Mass Spectrometry) U-Pb data from the Ouarzazate Group to better constrain the age progression related to the emplacement of the Ouarzazate Group pyroclastic rocks that record the large and fast paleomagnetic change in West Africa.

2. Geological context

The Anti-Atlas belt, situated in southern Morocco, represents the northern border of the West African craton (Fig. 2a) during the Neoproterozoic (Villeneuve and Cornée, 1994; Soulaimani et al., 2018). This mountain range is an ENE-trending lithospheric fold consisting of numerous inliers of Paleoproterozoic basement rocks overlain by Neoproterozoic/Paleozoic sedimentary and volcanic rocks (Fig. 2b). The upper Ediacaran sequences (~580-545 Ma) consist of a large volume of subaerial volcanic rocks, together with subordinate clastic sedimentary rocks, which unconformably overlie the older deformed Proterozoic rocks (Thomas et al. 2004; Gasquet et al. 2008; Blein et al., 2014a, b). These Ediacaran rocks are referred to as the Ouarzazate Group (Thomas et al. 2002) and are recognized in many inliers of the Anti-Atlas belt (Fig. 2b) with thicknesses reaching up to 2000m. The geodynamic explanation for the emplacement of the Ouarzazate Group along the NW margin of West Africa is still unclear. It has been proposed to be related to post-orogenic collapse (Thomas et al., 2002), a metacratonic event with igneous activity (Gasquet et al. 2008), oceanic subduction beneath thickened continental crust (Benziane, 2007), ridge-trench collision followed by a slab window (Blein et al. 2014a) or the emplacement of a large igneous province (Youbi et al. 2020).

Blein et al. (2014b) subdivided the Ouarzazate Group into four formations in the inliers of Agadir Melloul and Iguerda and in the southern side of the Sirwa inlier: (from the bottom to top in stratigraphic order) the Adrar-n-Takoucht, Anammar, Tadoughast and Fajjourd formations. U-Pb SHRIMP zircon ages obtained in these formations constrain the age of emplacement of the Ouarzazate Group in these inliers to between 572 and 556 Ma (Blein et al., 2014b). The large change in paleomagnetic directions reported by Robert et al. (2017) occurred between the emplacement of the Adrar-n-Takoucht and the Tadoughast formations. In this study, we identify three key sections to seek new high-resolution geochronologic constraints to determine more precisely the rate of these paleomagnetic changes (Fig. 2c, 3). Section 1 lies in south Sirwa, and the two other sections are in the Agadir Melloul inlier with Section 2 near the Aït Hamd locality and Section 3 close to the Jbel Iguiguil.

Section 1 is at the eastern tip of an anticline (called Adrar-n-Takoucht anticline in Robert et al. 2017) located on the southern side of the Sirwa inlier where the Adrar-n-Takoucht Formation unconformably overlies the early Ediacaran sedimentary rocks and locally volcanics of the Wawkida Group and unconformably underlies the Tadoughast and Fajjoud formations (Fig. 2c, 3). The Adrar-n-Takoucht Formation is mainly identified in this sector and consists of three distinct volcanic sequences separated by slight angular unconformities. The base of each sequence comprises a succession of massive ignimbrites overlain by more or less welded lithic, crystalline, hyaline tuffs and well-stratified cinerites. A sample from the basal ignimbrites of the first sequence yielded a U-Pb SHRIMP zircon age of 572 ± 5 Ma (TBOB647; Blein et al., 2014b). The overlying Tadoughast Formation consists of lithic and crystalline tuffs interstratified with levels of ignimbrites. A sample from a crystal tuff located close to the contact with the Adrar-n-Takoucht Formation yielded a U-Pb SHRIMP zircon age of 565 ± 6 Ma (TBTB329; Blein et al., 2014b).

Section 2 is within a syncline and an anticline close to the village of Aït Hamd in the Agadir Melloul inlier (called the Agadir-Melloul syncline/anticline in Robert et al., 2017) (Fig. 2c). In this sector, the Adrar-n-Takoucht is very thin and consists solely of a rhyolite overlying the deformed sedimentary rocks of the Wawkida Group. This rhyolite yielded a U-Pb SHRIMP zircon age of 570 ± 6 Ma (AMTB059; Blein et al., 2014b). The rhyolite is overlain by a chaotic breccia mapped as the Anammar Formation, and the Tadoughast Formation, which lies conformably on top of it. The Tadoughast Formation consists of alternating coarse to thin pyroclastic tuffs topped by thick plurimetric ignimbrites marking the highest levels of the formation. An andesite flow from the lower part of the formation yielded a U-Pb SHRIMP zircon age of 566 ± 6 Ma (AMTB061; Blein et al., 2014b). The Fajjoud Formation, which overlies the Tadoughast Formation with a slight unconformity, is a similar volcanic sequence consisting of crystalline and lithic tuffs topped by thick pyroclastic flows. One of the ignimbrites yielded a U-Pb SHRIMP zircon age of 556 ± 5 Ma (AMTB065; Blein et al., 2014b).

Section 3 is located in the northwestern border of the Agadir Melloul-Jbel Iguiguil inlier (Fig. 2c). In this sector, the basal Ouarzazate Group consists of the terrigenous sedimentary and volcanosedimentary rocks of the Anammar Formation unconformably overlying the Paleoproterozoic basement (Fig. 3). The Tadoughast Formation conformably overlies the Anammar Formation and consists, as in Section 2, of crystalline, lithic and hyaline pyroclastic tuffs topped by thick ignimbrites. The thick ignimbritic levels can be traced out and correlated within the entire Agadir Melloul inlier and therefore represent a robust stratigraphic marker. Samples from two grey welded ignimbrites located in the northern and southern borders of the Agadir Melloul-Jbel Iguiguil inlier yielded U-Pb SHRIMP zircon ages of 565 ± 5 Ma (TBOB063; Blein et al., 2014b) and 567 ± 5 Ma (AMOB211; Blein et al. 2014b). Additionally, a rhyolitic dome of the Tadoughast Formation sampled in the Agadir Melloul-Jbel Iguiguil yielded a U-Pb SHRIMP age of 564 ± 6 Ma (TBOB047; Blein et al., 2014b). Collectively with the age constraints from the south Sirwa inlier, it indicates emplacement of the Tadoughast Formation at around 567-564 Ma.

In this study, we dated seven samples using the U-Pb CA-ID-TIMS method on zircon to better characterize the rate of the paleomagnetic changes occurring between the emplacement of the Adrar-n-Takoucht and the Tadoughast formations. Three samples come from the Adrar-n-Takoucht Formation and four from the Tadoughast Formation distributed in Sections 1, 2 and 3 (Fig. 3). Because the large paleomagnetic excursion is observed in rocks from those sections, these samples can provide tighter constraints on the rate of the paleomagnetic changes.

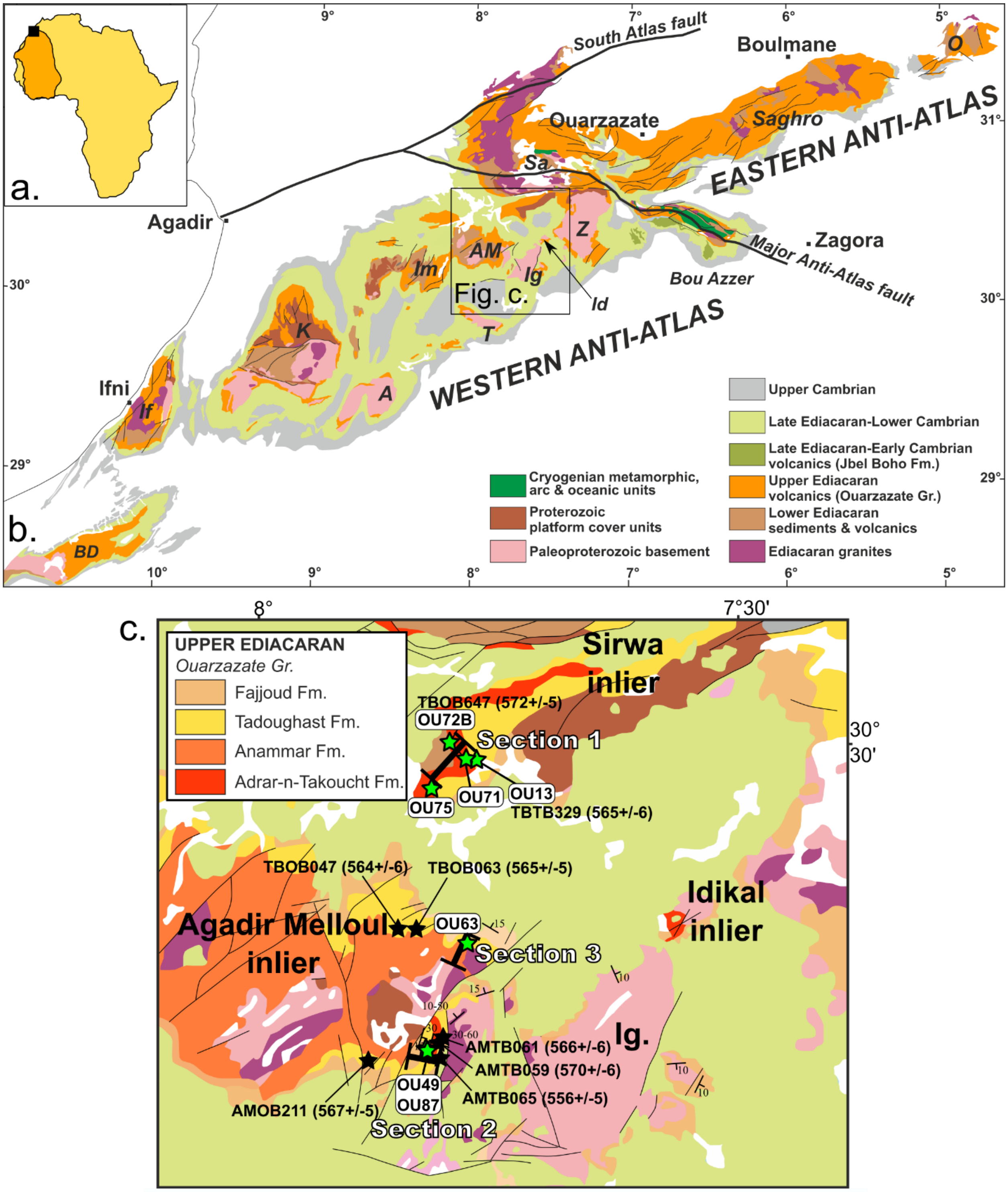

Figure 2: *a. Position of the West African craton (orange) within Africa (yellow). b. Geological map of the Anti-Atlas. Modified from Hollard et al. (1985), Walsh et al. (2002), Gasquet et al. (2008), Blein et al. (2014b) and Robert et al. (2017). Abbreviations: BD: Bas Drâa; If: Ifni; K: Kerdous; A: Tagragra d'Akka; Im: Igherm; T: Tagragra de Tata; Ig: Iguerda; Id: Idikal; AM: Agadir-Melloul; Sa: Sirwa; O: Ougnat. c. Zoom-in on the studied area: Agadir Melloul and Sirwa inliers. Location of the studied samples (green stars). Ages (+/- 2σ) previously obtained using U-Pb SHRIMP (zircon) by Blein et al. (2014b) (black stars).*

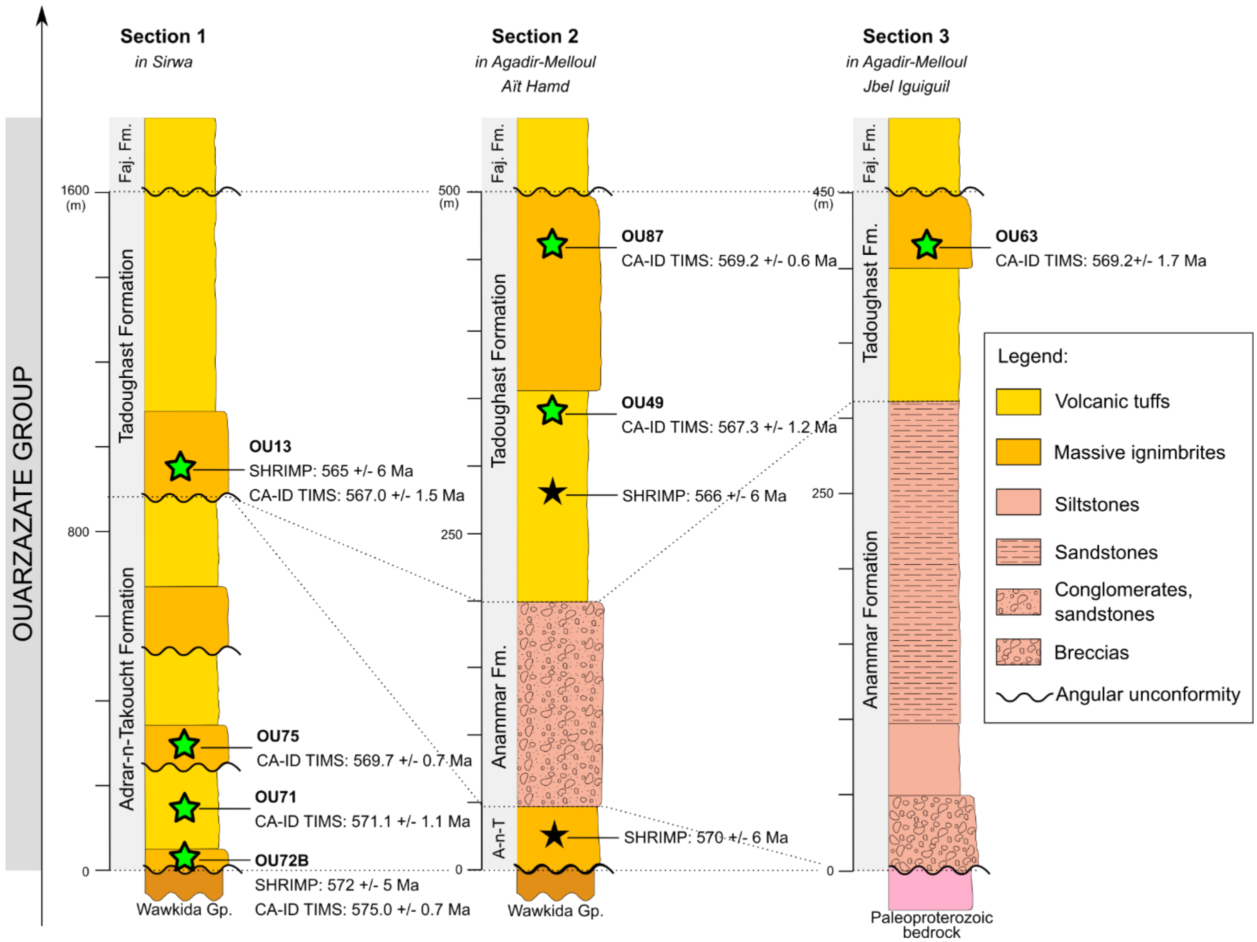

Figure 3: *Stratigraphic columns of the three studied sections (also shown in Fig. 2). Samples newly dated by CA ID-TIMS method shown by green stars. Samples dated by SHRIMP method displayed by black stars (Blein et al. 2014b). Uncertainties given with 2σ.*

3. Methods

Samples were crushed and pulverized, and then subjected to a series of heavy mineral concentration steps using a Wilfley table, sieving, magnetic separation, and heavy liquid flotation. The minerals were then hand-picked under a binocular microscope and subjected to chemical abrasion (Mattinson, 2005). Dissolution of the zircons was done in Krogh-type bombs at 195 °C, after addition of a mixed ^{202}Pb–^{205}Pb–^{235}U spike. The spike was calibrated with reference to a ^{206}Pb/^{238}U value of 0.0156513 for the ET100 solution. Fractionation was monitored by daily measurements of the NBS982 and U500 standard solutions, and regular analyses of reference material such as 91500 zircon (Wiedenbeck et al., 1995). The ID-TIMS process is based on Krogh (1973). A more specific description of the procedure used in the Oslo laboratory is given in Corfu (2004). The data were corrected for blanks of 2 pg Pb and 0.1 pg U and calculated using the decay constants of Jaffey et al. (1971) and ^{238}U/^{235}U = 137.88. Initial Pb was corrected using compositions taken from Stacey and Kramers (1975). Plotting and calculation were done with Isoplot (Ludwig, 2009).

4. Results

4.1. The Adrar-n-Takoucht Formation

The analyses performed on the samples from the Adrar-n-Takoucht Formation are all from Section 1. The samples have the same labels as the paleomagnetic sites where they were collected (in stratigraphic order): OU72B, OU71A and OU75.

Sample OU72B is from an ignimbrite, described in Blein et al. (2014b) as a rhyolitic crystal tuff (TBOB647) containing quartz and feldspar crystal clasts, some lithic clasts derived from trachytic lavas, and ignimbrites shards. Zircon grains extracted from this sample are mostly short-prismatic to equant, mostly euhedral and with local inclusions and alteration (Fig. 4a). The analyses were done on some of the best euhedral crystals and tips after chemical abrasion. Seven out of the eight zircon analyses are concordant and yielded $^{206}Pb/^{238}U$ dates ranging from 575.2 to 566.8 Ma, and one zircon analysis is slightly discordant and gave a date of 564.9 (Table 1 and Fig. 5a). The three older dates are very consistent with each other and yielded a mean $^{206}Pb/^{238}U$ age of 575.0 ± 0.8 Ma (MSWD = 0.16). The five other dates spread down to 564 Ma, likely due to Pb loss.

Sample OU71A is from a series of well-stratified ashy tuffs. Only a few zircon grains were found in the sample. Most grains are short prismatic to equant but there are few elongated tips (Fig. 4b). Among the seven analyses (Fig. 5b), four concordant data points and one slightly discordant result gave consistent $^{206}Pb/^{238}U$ dates ranging from 572.3 to 570.1 Ma, and yielded a mean $^{206}Pb/^{238}U$ age of 571.1 ± 1.1 Ma (MSWD = 1.4). The two remaining dates are slightly discordant and have their ellipse of 95% confidence only partially crossing the other five results. The older discrepant analysis could correspond to an antecrystic grain, while the younger one likely reflects some Pb loss, and these two data points were therefore discarded from the age calculation.

Sample OU75 is from a massive ignimbrite and consists of a fine matrix with submillimetric welded crystalline clasts. The sample yielded a fairly abundant zircon population, generally consisting of elongated prisms but also with some more equant grains (Fig. 4c). Inclusions and some alteration are seen in most of the grains. One of the zircon grains yielded a $^{206}Pb/^{238}U$ date of 621.2 Ma, which is much older than the presumed age of the rock and is probably an inherited zircon. The other eleven analyses are concordant with $^{206}Pb/^{238}U$ dates ranging from 570.6 to 563.5 Ma (Fig. 5c). The distribution of dates displays three plateaus at ca. 570 Ma, ca. 567 Ma and ca. 565 Ma (Fig. 7), which renders the determination of the age of emplacement for this pyroclastic rock difficult. We tentatively calculated two $^{206}Pb/^{238}U$ ages, a first one using the three older grains yielding an age of 569.7 ± 0.7 Ma, and a second one by grouping all the remaining dates that are quite close in age giving an age of 565.2 ± 0.6 Ma. The existence of these two equally viable ages might be explained by slight Pb loss and/or by the presence of antecrysts. The significance of these two ages will be evaluated in the next section using information given by stratigraphy.

4.2. The Tadoughast Formation

The analyses performed on the samples from the Tadoughast Formation are from all three sections and have the same labels as the corresponding paleomagnetic sites (in stratigraphic order): OU13, OU49, OU87 and OU63.

Sample OU13 is defined as a crystal-rich pyroclastic tuff in Blein et al. (2014b) (TBTB329) and comprises crystal clasts (< 1mm) with a diffuse layering locally outlined by millimeter scale crystal clasts with a vitroclastic texture. The zircon population is quite uniform and dominated by prisms with prominent {211} pyramids, but mostly with inclusions and rich in U (Fig. 4d). Among the eight zircon analyses, one is strongly discordant (Disc = 46.1%; Table 1); the grain probably had an inherited core and the analysis projects to an age of 2190 Ma. Of the seven remaining results, three concordant analyses yielded $^{206}Pb/^{238}U$ dates consistent with each other within uncertainty at 568.0, 567.4 and 566.1 Ma. Another $^{206}Pb/^{238}U$ date of 566.2 Ma is slightly discordant but has its ellipse of 95% confidence crossing the other three. These four results define a mean $^{206}Pb/^{238}U$ age of 567.0 ± 1.5 Ma (Fig. 6a). The three remaining dates have their ellipse of 95% confidence distinct from the three well-defined analyses. While the two younger ones could be affected by Pb loss, the older one, with a $^{206}Pb/^{238}U$ date of 571.4 Ma, could correspond to an antecryst or inherited zircon.

Sample OU49 is from a red hyaline tuff with a greater proportion of shards than of crystal clasts. The extracted zircons are mostly equant to short prismatic but also include a few more elongated prisms and fragments (Fig. 4e). There are also some more rounded grains, which were excluded from the initial selection. Two of the six analyzed zircons yielded inherited Paleoproterozoic, nearly concordant $^{207}Pb/^{206}Pb$ dates of 2040.3 Ma and 2036.2 Ma. Two zircons gave early Ediacaran inherited $^{206}Pb/^{238}U$ dates at 616.4 Ma and 595.9 Ma. The two last grains yielded $^{206}Pb/^{238}U$ dates at 572.8 Ma and 567.0 Ma, with the former result being slightly discordant. Overall, the dataset from sample OU49 is poorly defined due to the extensive presence of xenocrysts. We tentatively interpret the youngest date as being representative of the time of extrusion, yielding a $^{206}Pb/^{238}U$ age of 567.3 ± 1.2 Ma.

Sample OU87 is from a massive grey ignimbrite, consisting of a grey-purple recrystallized matrix of hyaline and slightly eutaxitic texture and some clasts of quartz and feldspars. The sample yielded zircon grains consisting of both long-prisms and short to equant grains. Most of the grains have some inclusions (Fig. 4f, i). Among the nine analyses, only one is slightly discordant and yielded a $^{206}Pb/^{238}U$ date of 572.3 Ma. The eight other results yielded very consistent $^{206}Pb/^{238}U$ dates ranging from 570.8 to 567.8 Ma, with a mean age of 569.6 ± 0.9 Ma (MSWD = 2.1) (Fig. 6b). A MSWD score closer to 1 can be achieved if the oldest concordant and slightly outlying result is discarded, giving a mean age of 569.2 ± 0.6 Ma (MSWD = 0.64).

Sample OU63 is from a massive grey ignimbrite and is similar to sample OU87 with a lower proportion of crystal clasts. The zircon population was abundant and dominated by euhedral crystals both long and short prismatic, but most grains contained inclusions (Fig. 4g, h). The ten analyses are concordant but yield a spread in $^{206}Pb/^{238}U$ dates ranging from 570.1 Ma to 564.1 Ma (Fig. 6c). As in sample OU75, the large spread of concordant results renders the determination of an accurate age difficult. We again calculated two mean $^{206}Pb/^{238}U$ ages, an older one using the four oldest dates and a second one when taking the six youngest dates. The obtained mean ages are respectively 569.2 ± 1.7 Ma (MSWD = 2.0) and 565.7 ± 1.3 Ma (MSWD = 2.4). We recognize that this selection is arbitrary but it allows bracketing the age of the rock between the two end-member mean dates.

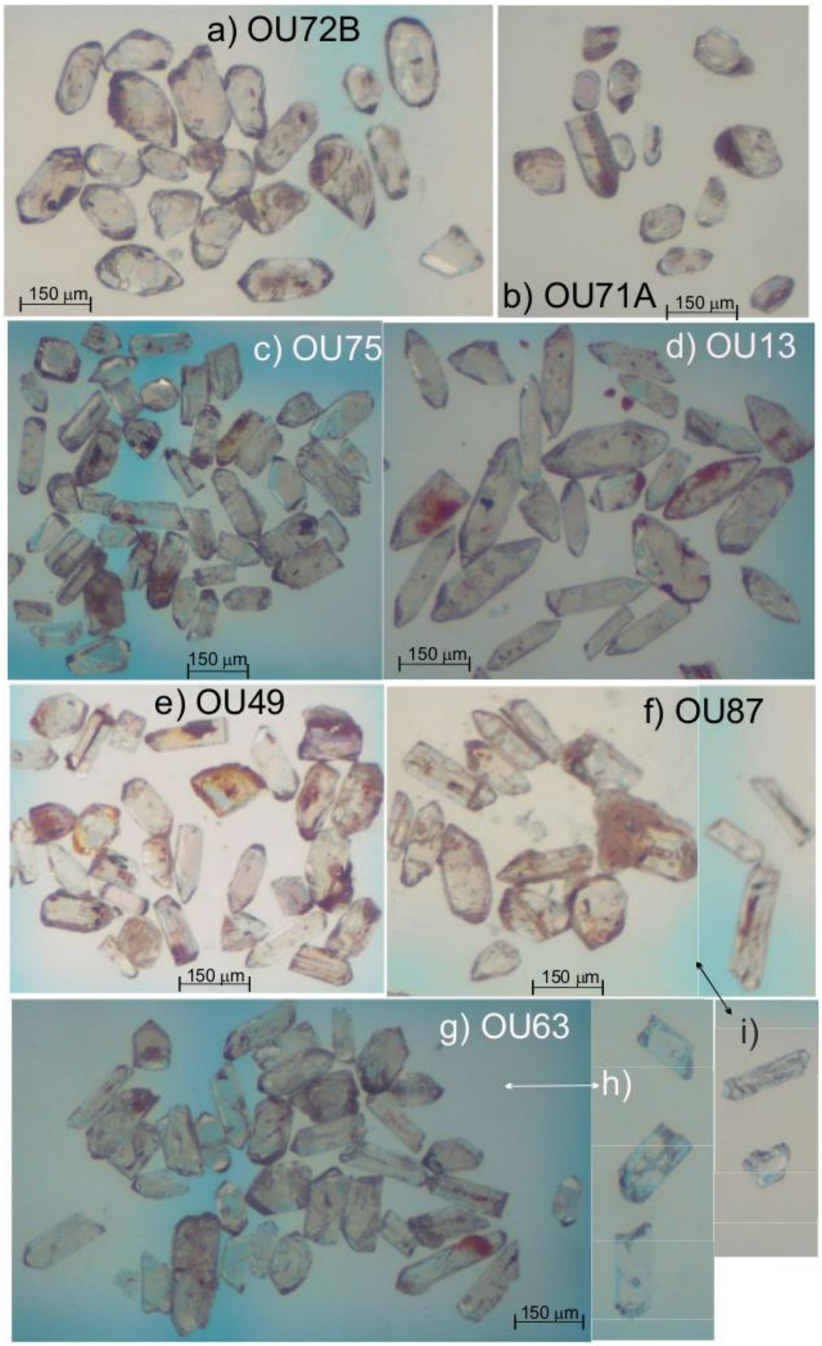

Figure 4 *: Zircon grains selected for annealing and chemical abrasion from the various samples. Some of the grains still have partial coatings of volcanic glass or are rusty, and many have inclusions of other minerals and/or local alteration. These features were dissolved away by the chemical abrasion treatment, but some of the grains became partially cloudy. Typical appearances after chemical abrasion are shown in (h) representing grains of sample OU63 and (i) representing grains of OU87.*

Table 1. U-Pb data

Zircon features[1]	Weight [ug][2]	U [ppm][2]	Th/U[3]	Pbc[4] [pg]	^{206}Pb/^{204}Pb[5]	^{207}Pb/^{235}U[6]	2 σ [abs]	^{206}Pb/^{238}U[6]	2 σ [abs]	rho	^{207}Pb/^{206}Pb[6]	[abs]	^{206}Pb/^{238}U[6] [Ma]	2 σ [abs]	^{207}Pb/^{235}U[6] [Ma]	2 σ [abs]	^{207}Pb/^{206}Pb[6] [Ma]	2 σ [abs]	D[7] [%]
OU72B Ignimbrite Adrar-n-Takoucht formation																			
sp	2	407	0.3	1.3	3625	0.762	0.002	0.09333	0.00020	0.79	0.05922	0.00011	575.2	1.2	575.2	1.4	575.2	4.1	0.0
tip	1	193	0.3	0.5	2185	0.762	0.003	0.09332	0.00025	0.80	0.05921	0.00013	575.1	1.4	575.1	1.6	575.0	4.7	0.0
tip	1	495	0.3	1.2	2351	0.763	0.002	0.09325	0.00022	0.83	0.05931	0.00011	574.7	1.3	575.5	1.4	578.6	4.0	0.7
sp	1	411	0.2	0.5	4796	0.755	0.003	0.09286	0.00028	0.83	0.05898	0.00014	572.4	1.7	571.2	1.8	566.4	5.0	-1.1
sp	2	347	0.2	0.9	3461	0.754	0.002	0.09263	0.00020	0.83	0.05907	0.00010	571.0	1.2	570.8	1.3	569.6	3.6	-0.3
sp	1	793	0.2	0.7	6412	0.753	0.003	0.09230	0.00032	0.88	0.05914	0.00012	569.1	1.9	569.7	1.8	572.1	4.2	0.5
sp	1	265	0.2	0.8	1914	0.749	0.003	0.09190	0.00025	0.88	0.05909	0.00010	566.8	1.5	567.5	1.5	570.5	3.5	0.7
sp	1	414	0.2	1.3	1813	0.741	0.003	0.09158	0.00024	0.79	0.05865	0.00013	564.9	1.4	562.8	1.6	554.1	4.9	-2.0
OU71A Tuff Adrar-n-Takoucht formation																			
tip	1	240	0.3	1.1	1281	0.762	0.003	0.09309	0.00026	0.79	0.05937	0.00014	573.8	1.5	575.2	1.7	580.7	5.2	1.2
lp-tip	1	57	0.4	1.1	298	0.754	0.006	0.09283	0.00028	0.51	0.05890	0.00039	572.3	1.6	570.5	3.3	563.3	14.4	-1.7
sp	1	138	0.3	0.6	1353	0.753	0.003	0.09274	0.00023	0.78	0.05888	0.00014	571.7	1.4	569.9	1.6	562.6	5.1	-1.7
tip	1	405	0.3	0.5	4470	0.754	0.002	0.09265	0.00023	0.87	0.05903	0.00009	571.2	1.4	570.6	1.4	568.3	3.3	-0.5
tip	1	103	0.2	0.4	1399	0.752	0.003	0.09252	0.00023	0.77	0.05897	0.00014	570.4	1.3	569.5	1.6	566.1	5.1	-0.8
lp-fr	1	174	0.4	0.5	1964	0.755	0.003	0.09246	0.00025	0.71	0.05920	0.00018	570.1	1.5	571.0	1.9	574.5	6.6	0.8
tip	1	295	0.3	0.6	2769	0.747	0.002	0.09226	0.00021	0.80	0.05876	0.00012	568.9	1.3	566.7	1.4	558.0	4.3	-2.0
OU75 Ignimbrite Adrar-n-Takoucht formation																			
sp	1	525	0.6	1.9	1801	0.843	0.003	0.10117	0.00026	0.81	0.06042	0.00012	621.2	1.5	620.6	1.6	618.5	4.4	-0.5
lp-fr	2	144	0.3	1.8	941	0.753	0.005	0.09255	0.00028	0.58	0.05901	0.00030	570.6	1.7	569.9	2.7	567.3	11.0	-0.6
tip	2	1202	0.2	2.9	4890	0.752	0.002	0.09233	0.00019	0.87	0.05905	0.00008	569.3	1.1	569.3	1.1	569.1	2.8	0.0
fr	1	2298	0.3	1.7	8036	0.752	0.002	0.09239	0.00020	0.90	0.05906	0.00007	569.6	1.2	569.6	1.1	569.2	2.5	-0.1
tip	1	136	0.5	0.8	1047	0.748	0.004	0.09198	0.00028	0.75	0.05901	0.00020	567.2	1.6	567.3	2.2	567.4	7.4	0.0
lp-tip	7	269	0.6	2.5	4315	0.747	0.002	0.09196	0.00020	0.83	0.05892	0.00010	567.1	1.2	566.5	1.3	564.1	3.6	-0.6
tip	1	796	0.2	1.7	2726	0.748	0.002	0.09194	0.00021	0.84	0.05900	0.00010	567.0	1.3	567.1	1.3	567.2	3.7	0.0
lp-fr	1	353	0.5	1.9	1073	0.747	0.005	0.09175	0.00038	0.66	0.05903	0.00031	565.8	2.2	566.3	3.1	568.2	11.5	0.4
tip	1	1148	0.2	1.4	4783	0.747	0.002	0.09169	0.00021	0.81	0.05911	0.00011	565.5	1.2	566.6	1.3	571.1	4.0	1.0
sp	2	395	0.2	1.2	3725	0.743	0.003	0.09168	0.00020	0.72	0.05878	0.00014	565.5	1.2	564.2	1.5	559.1	5.1	-1.2
tip	1	780	0.2	2.8	1630	0.745	0.002	0.09159	0.00022	0.84	0.05897	0.00010	564.9	1.3	565.2	1.3	566.2	3.7	0.2
lp-fr	5	19	0.3	1.9	316	0.742	0.009	0.09135	0.00034	0.53	0.05891	0.00062	563.5	2.0	563.6	5.1	563.7	22.6	0.0
OU13 Tuff Tadoughast formation																			
tip	1	720	1.8	1.5	3934	1.570	0.007	0.12922	0.00055	0.94	0.08809	0.00014	783.4	3.1	958.2	2.9	1384.5	3.0	46.1
sp	2	353	0.3	1.4	2978	0.759	0.003	0.09269	0.00020	0.68	0.05938	0.00016	571.4	1.2	573.3	1.6	581.0	5.7	1.7
sp	1	1146	0.2	1.3	5159	0.748	0.002	0.09211	0.00022	0.84	0.05890	0.00010	568.0	1.3	567.1	1.4	563.4	3.7	-0.8
tip	1	650	0.2	2.4	1608	0.749	0.004	0.09200	0.00027	0.64	0.05908	0.00025	567.4	1.6	567.9	2.4	570.2	9.3	0.5
sp	1	505	0.2	5.8	522	0.742	0.004	0.09181	0.00024	0.61	0.05862	0.00025	566.2	1.4	563.6	2.4	553.0	9.4	-2.5
lp	1	778	0.2	4.9	940	0.746	0.003	0.09179	0.00029	0.76	0.05898	0.00018	566.1	1.7	566.1	2.0	566.2	6.5	0.0
sp	1	874	0.2	0.9	5611	0.736	0.005	0.09132	0.00058	0.91	0.05849	0.00018	563.3	3.4	560.3	3.2	548.0	6.6	-2.9
sp	1	1566	0.2	1.0	8806	0.737	0.005	0.09081	0.00049	0.85	0.05886	0.00020	560.3	2.9	560.6	2.9	562.0	7.5	0.3
tip	1	381	0.2	1.4	1543	0.722	0.002	0.08898	0.00020	0.77	0.05889	0.00012	549.5	1.2	552.1	1.4	562.9	4.6	2.5
OU49 Tuff Tadoughast formation																			
lp-fr	2	526	0.2	3.2	5608	6.441	0.022	0.37128	0.00118	0.98	0.12582	0.00010	2035.4	5.5	2037.8	3.0	2040.3	1.3	0.3
tip	1	211	0.4	3.7	1309	6.401	0.028	0.36984	0.00145	0.93	0.12552	0.00020	2028.6	6.8	2032.4	3.8	2036.2	2.8	0.4
lp-fr	2	160	0.6	1.3	1593	0.835	0.005	0.10112	0.00027	0.55	0.05989	0.00031	621.0	1.6	616.4	2.9	599.5	11.3	-3.8
sp	1	405	0.6	0.7	3529	0.798	0.004	0.09601	0.00034	0.84	0.06031	0.00014	591.0	2.0	595.9	2.0	614.6	5.1	4.0
lp-fr	2	583	0.4	1.8	3715	0.758	0.002	0.09268	0.00020	0.91	0.05931	0.00007	571.4	1.2	572.8	1.2	578.5	2.4	1.3
tip	1	1317	0.2	0.6	11820	0.748	0.002	0.09198	0.00021	0.94	0.05897	0.00005	567.3	1.2	567.0	1.1	565.9	2.0	-0.3
OU87 Ignimbrite Tadoughast formation																			
eq	3	170	0.2	0.9	3380	0.757	0.002	0.09318	0.00022	0.82	0.05892	0.00011	574.3	1.3	572.3	1.4	564.2	4.0	-1.9
sp	3	187	0.4	2.3	1432	0.754	0.003	0.09276	0.00024	0.76	0.05899	0.00016	571.8	1.4	570.8	1.8	566.7	5.8	-1.0
lp	1	357	0.4	0.7	2810	0.754	0.004	0.09259	0.00036	0.86	0.05910	0.00015	570.8	2.1	570.8	2.1	570.9	5.4	0.0
lp	1	340	0.5	1.3	1481	0.751	0.002	0.09235	0.00022	0.85	0.05899	0.00009	569.4	1.3	568.8	1.3	566.6	3.5	-0.5
lp-tip	1	359	0.4	1.1	1972	0.753	0.003	0.09234	0.00025	0.80	0.05917	0.00014	569.4	1.5	570.2	1.7	573.3	5.0	0.7
tip	1	436	0.3	0.2	12021	0.751	0.002	0.09235	0.00023	0.83	0.05896	0.00011	569.4	1.4	568.7	1.4	565.7	3.9	-0.7
tip	1	424	0.4	2.5	992	0.753	0.003	0.09222	0.00024	0.78	0.05925	0.00014	568.6	1.4	570.2	1.7	576.4	5.2	1.4
lp	1	550	0.4	1.3	2433	0.751	0.005	0.09212	0.00054	0.93	0.05910	0.00014	568.1	3.2	568.6	2.8	570.8	5.0	0.5
lp-fr	3	56	0.4	1.0	969	0.749	0.005	0.09227	0.00021	0.55	0.05889	0.00031	569.0	1.3	567.8	2.7	563.2	11.4	-1.1
OU63 Ignimbrite Tadoughast formation																			
lp-fr	1	577	0.3	3.1	1092	0.752	0.003	0.09247	0.00025	0.80	0.05901	0.00013	570.1	1.5	569.6	1.6	567.4	4.9	-0.5
lp-fr	2	480	0.3	0.9	5883	0.752	0.003	0.09237	0.00020	0.71	0.05905	0.00014	569.6	1.2	569.5	1.5	569.1	5.3	-0.1
lp-fr	1	476	0.3	1.2	2235	0.747	0.004	0.09217	0.00031	0.65	0.05875	0.00027	568.4	1.8	566.2	2.6	557.8	9.8	-2.0
sp	1	1076	0.3	1.4	4551	0.747	0.003	0.09203	0.00031	0.88	0.05890	0.00012	567.5	1.9	566.7	1.8	563.6	4.3	-0.7
lp-tip	1	1047	0.3	1.5	3919	0.747	0.003	0.09194	0.00034	0.84	0.05894	0.00015	567.0	2.0	566.6	2.0	564.7	5.5	-0.4
sp	1	657	0.3	0.5	7097	0.748	0.002	0.09189	0.00024	0.87	0.05906	0.00010	566.7	1.4	567.2	1.4	569.3	3.5	0.5
tip	1	899	0.3	4.6	1148	0.746	0.003	0.09186	0.00026	0.83	0.05893	0.00012	566.5	1.5	566.1	1.6	564.3	4.5	-0.4
lp	1	1056	0.3	0.8	7356	0.748	0.005	0.09175	0.00036	0.66	0.05914	0.00031	565.9	2.1	567.1	3.0	572.1	11.3	1.1
lp-fr	1	697	0.3	1.4	2936	0.745	0.002	0.09158	0.00021	0.84	0.05898	0.00010	564.9	1.3	565.2	1.4	566.4	3.7	0.3
tip	1	776	0.2	1.2	3738	0.742	0.002	0.09145	0.00024	0.90	0.05888	0.00008	564.1	1.4	563.8	1.4	562.7	3.0	-0.2

[1] Zircon: all euhedral single grains and chemically abraded: eq = equant; sp = short-prismatic; lp = long prismtic; (lp-)tip = (long) tip of crystal; fr = fragment; lp-fr = piece of long prismatic crystal.
[2] weight and concentrations are known to better than 10-30%, depending on grain size
[3] Th/U model ratio inferred from 208/206 ratio and age of sample
[4] Pbc = total common Pb in sample (initial +blank)
[5] raw data corrected for fractionation and blank
[6] corrected for fractionation, spike, blank and initial common Pb; error calculated by propagating the main sources of uncertainty; initial common Pb estimated with the model of Stacey and Kramers (1975) for the age of the samples.
[7] D = degree of discordancy

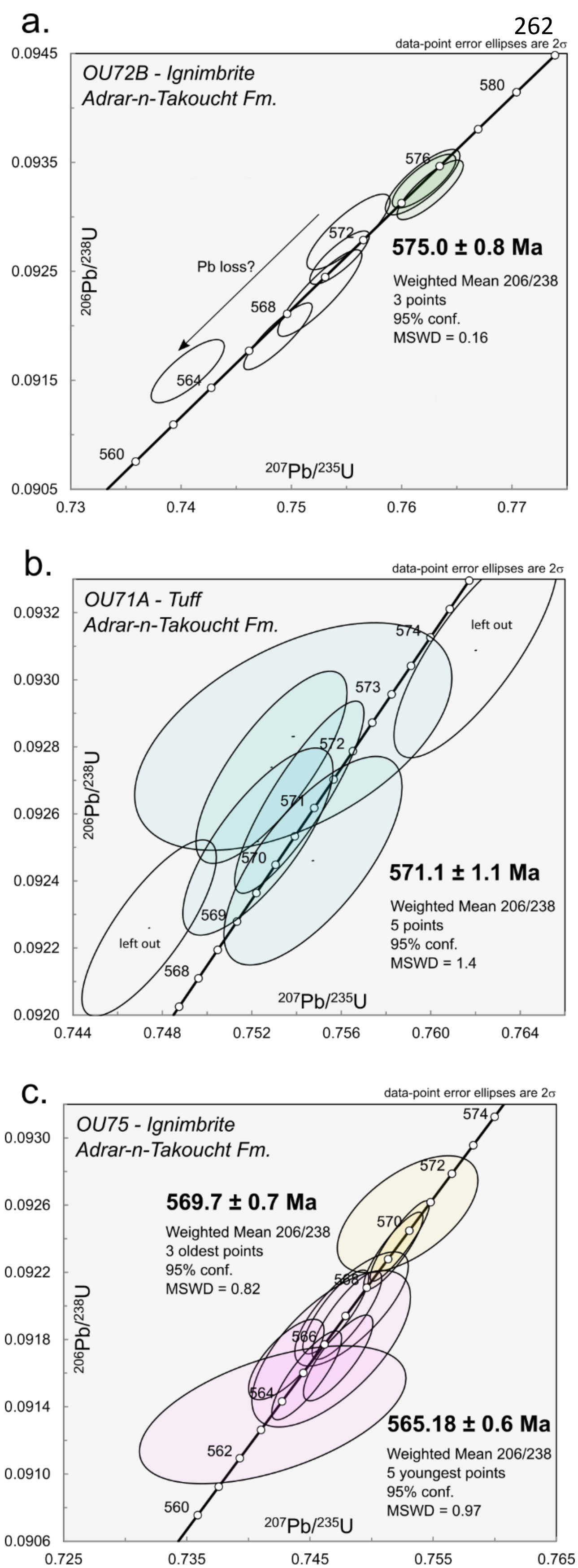

Figure 5: *Concordia diagrams displaying the zircon dates of the samples OU72B (a), OU71A (b) and OU75 (c) from the Adrar-n-Takoucht Formation. Colored ellipses are dates used for the calculation of the sample ages. In the case of OU75, two possible ages are calculated. See text for explanation about the data selection.*

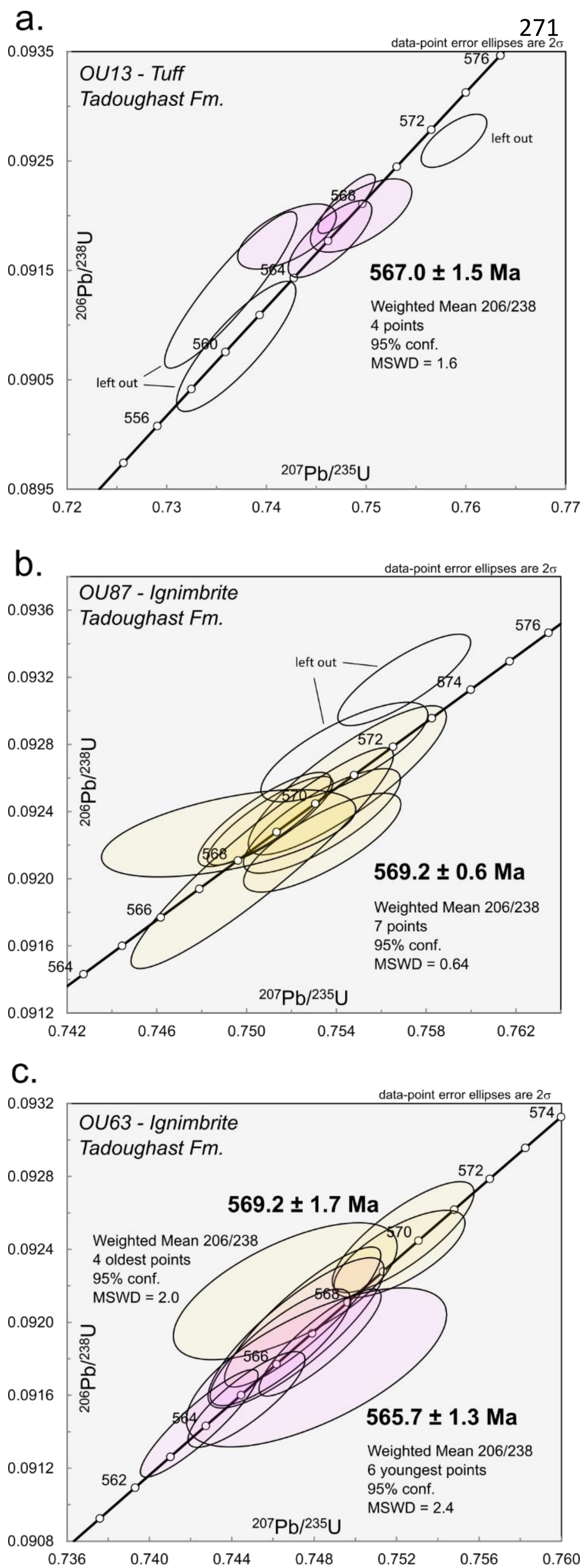

Figure 6: *Concordia diagrams displaying the zircon dates of the samples OU87 (a), OU63 (b) and OU13 (c) from the Tadoughast Formation. Colored ellipses are dates used for the calculation of the sample ages. In the case of OU63, two possible ages are calculated. See text for explanation about the data selection.*

5. Discussion

5.1. Inheritance and Pb loss

Multiple flare-up pulses characterize the volcanic activity of magmatic systems in continental arcs, which grow by the concurrent emplacement of large granitic/granodioritic plutons in the crust and the extrusion of voluminous pyroclastic rocks including thick ignimbrites (Da Silva et al., 2015). During magma ascent through the crust or locally during emplacement, various xenocrysts may be incorporated. The two Paleoproterozoic zircons (^{207}Pb/^{207}Pb dates of 2040.3 and 2036.2 Ma) found in sample OU49 in Section 2 represent the oldest xenocrysts identified in this study. The discordia line through one discordant date of sample OU13 yields an upper intercept age of 2190 Ma, indicating that the zircon grain contained a core of Paleoproterozoic age. Blein et al. (2014b) identified similar zircon ages within some of the Ouarzazate samples. Soulaimani et al. (2013) report Paleoproterozoic intrusions of that age in the Agadir Melloul inlier (Tazenacht suite). More generally, Paleoproterozoic dolerites and granites with ages ranging from ca. 2050 to 2000 Ma intrude and floor the Anti-Atlas belt (Gasquet et al., 2008) and represent a likely source for xenocrysts. We also identified xenocrystic zircons of early Ediacaran age in samples OU75 (^{206}Pb/^{238}U dates of 621.2 Ma) and OU49 (^{206}Pb/^{238}U dates of 616.4 Ma and 595.9 Ma). In the Sirwa inlier, Thomas et al. (2002) reported U-Pb ages ranging from 615 to 580 Ma from intrusions of the Assaragh Suite with the oldest, the Mzil granite, yielding a SHRIMP U-Pb age of 614 ± 10 Ma. The Assaragh suite could be a possible source for the xenocryst identified in sample OU75. In the Agadir Melloul inlier where we collected sample OU49, very few early Ediacaran rocks have been identified. They correspond to the sedimentary rocks of the Wawkida Group. Numerous dolerites intrude the Paleoproterozoic inliers and notably the Jbel Iguiguil inlier, which is next to sections 2 and 3. One of the dolerites yielded a SHRIMP U-Pb age of 570 ± 7 Ma, younger than the xenocrysts found in sample OU49. The origin of these zircons remains unclear.

It is also common in magmatic systems that zircon grains which crystalized during early pulses of magmatism become incorporated in later magmas (Miller et al. 2007). These grains, called antecrysts, are generally similar in composition to the autocrysts, which crystallized in the last pulse and correspond to the age of emplacement. The Ouarzazate Group was formed by the accumulation of magma produced in many pulses from ~572 to 556 Ma (Blein et al., 2014b), and samples may contain antecrysts. The Ouarzazate Group unconformably overlies early to mid-Ediacaran rocks (Wawkida Fm), which are associated with a magmatic phase that erupted ~20 Myrs before the emplacement of the Ouarzazate Group. The Adrar-n-Takoucht Formation corresponds to the first pulse of the Ouarzazate Group, and therefore the base of the formation should not contain antecrysts. It is therefore reasonable to consider that the older mid-Ediacaran grains in OU72B correspond to the emplacement of the ignimbrite at ~575 Ma. Samples positioned higher in the stratigraphy, except for the xenocrysts discussed above, have no zircons older than 575 Ma and corroborate this notion. More generally, because the proportion of autocrysts relative to antecrysts depends on various parameters (Zr content, alkalinity, magma mixing) that are difficult to determine, the information given by stratigraphy is crucial to assess whether the mean age reflects the age of emplacement.

A mean age is usually defined by an age plateau. However, some samples show no real plateau but a continuous spread toward younger ages that could be due to Pb loss. After the emplacement of the rock, Pb loss can occur in crystal lattices that have been damaged, allowing for the diffusion of Pb (Schoene, 2014). Damage is induced by the disintegration of U and Th and results from alpha recoil and fission track accumulation, or by crystal plastic deformation. We treated our samples with chemical abrasion, which eliminates or at least limits the effects of Pb loss by dissolving the discordant domains in the crystal lattices

(Mattinson, 2005). In the Anti-Atlas belt, Rb-Sr, K-Ar, zircon fission track analyses, and pervasive paleomagnetic remagnetization (Charlot, 1976; Bonhomme and Hassenforder, 1985; Sebti et al., 2009; Boudzoumou et al., 2012; Robert et al., 2017) reveal a low-grade thermal metamorphic event (up to ~350°C) associated with the Hercynian orogeny in the Carboniferous and Permian. This event could be responsible for Pb loss by enhancing the diffusion of Pb in damaged crystal lattices. Because this potential age of U-Pb system opening is close to the age of emplacement of the studied rocks, it is not possible to test this hypothesis using discordia arrays because these are parallel to the Concordia curve. Consequently, a grain that yields a concordant analysis might still be affected by Pb loss. In this context, a key characteristic for the identification of Pb loss resides in the distribution of dates within samples: a plateau will rather define the age of emplacement while a continuous spread would rather suggest Pb loss. For some of the samples, this spread is evident, such as in samples OU72B and OU13 (Fig. 5a, 6c). For others, the age distribution is rather bimodal, such as in samples OU75 and OU63, and could reflect Pb loss, the presence of antecrysts or a combination of the two.

5.2. Age progression with stratigraphy

In the following, we will discuss the consistency of these new ages with the stratigraphic framework that has previously been established (Blein et al., 2014b).

In Section 1, three samples are from the Adrar-n-Takoucht Formation and one sample is from the Tadoughast Formation (Fig. 3). Samples OU72B, OU71A and OU13 yielded ages consistent with stratigraphy with an age-progression of 575.0 ± 0.8 Ma, 571.1 ± 1.1 Ma and 567.0 ± 1.5 Ma respectively. In sample OU75, we were not able to define a unique solution and we defined two possible ages: 569.7 ± 0.7 Ma and 565.2 ± 0.6 Ma. The first age determination is consistent with the age evolution given by the other samples, whereas the second result is too young. As discussed above, Pb loss would tend to drive dates toward younger ages and might explain why there are some zircons in OU75 yielding too young dates.

In Section 2, two samples were analyzed, both coming from the Tadoughast Formation. Sample OU49 yielded poorly defined results, and is tentatively dated at 567.3 ± 1.2 Ma using the youngest zircon date. This age is inconsistent with the age of 569.2 ± 0.6 Ma given by sample OU87 located stratigraphically above, at the top of the Tadoughast Formation. This age is very well determined by seven dates and we think it is more robust than the age given by OU49 obtained from only one zircon analysis, and we therefore discard the result from OU49 in the following.

In Section 3, only one sample has been analyzed from the Tadoughast Formation (OU63). Results were ambiguous as two approximately different groups of dates could represent the age of emplacement at 569.2 ± 1.7 Ma and 565 ± 1.3 Ma. Sample OU63 is from one of the massive ignimbrites capping the Tadoughast Formation and should have a similar age as OU87. The first age determination would then fit very well with the age of sample OU87. An additional time constraint is from the paleomagnetic data that show that there was at least one magnetic reversal in between the emplacement of these two ignimbrites (Robert et al., 2017). Reversal rates for the late Neoproterozoic have been the subject of many studies and were likely very high with 10 to 20 reversals occurring per Myr (Halls et al., 2015; Bazhenov et al., 2016; Levashova et al., 2021). If such a rate was at play during the mid-Ediacaran, a reversal should occur every 50 to 100 kyrs. Such a period is about one order of magnitude below the uncertainties of our results and therefore paleomagnetism cannot further inform our age interpretation.

Combining the results from the three sections allows refinement of the emplacement age of the Tadoughast Formation. The base and top of the formation are, respectively, constrained at 567 ± 1.5 Ma (Sample OU13) and 569.2 ± 0.7 Ma (Sample OU87). These two ages are similar when taking the maximum uncertainties of each result at 568.5 Ma. However, the age of sample OU87 is more robust because it is constrained by an age plateau containing more dates, and so an age of 569.2 Ma is likely more representative for the emplacement of the Tadoughast Formation. In any case, these new constraints support the emplacement of the Tadoughast Formation during a very short amount of time within about 1-2 Myrs. Previous SHRIMP age constraints obtained in the Agadir Melloul inlier and the south Sirwa yielded mean ages around 567-564 Ma, which are slightly younger than the one obtained in this study. Similarly, our new constraints for the Adrar-n-Takoucht Formation define a basal age 3 Myrs older than that previously estimated by Blein et al. (2014b). These differences could originate from the better removal of Pb loss with the CA-ID-TIMS method.

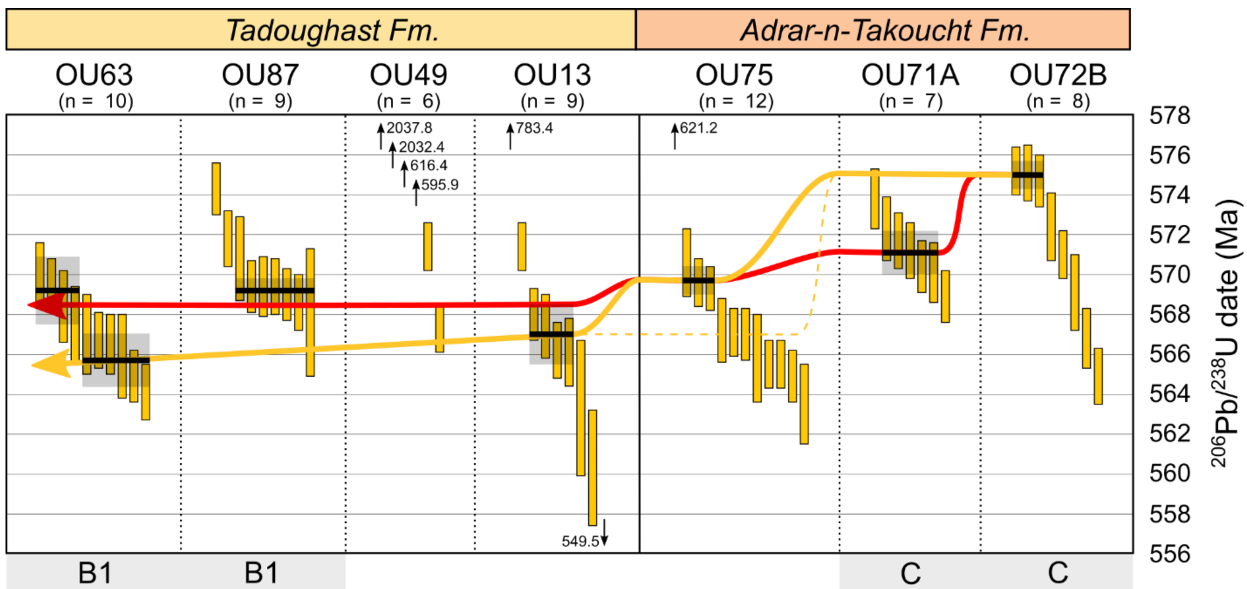

__Figure 7:__ Alternative age progressions (yellow or red) for the emplacement of the volcanic successions from the Adrar-n-Takoucht and Tadoughast formations. For each sample, U-Pb dates obtained from zircons are displayed as yellow bars (spanning 2σ uncertainties). Weighted mean results are shown as black lines associated with uncertainties (2σ) as grey band. The paleomagnetic component recorded in samples (B1 or C) is also displayed.

5.3. Estimates of the rate of change

Based on the new geochronological constraints on the Adrar-n-Takoucht and Tadoughast formations, we define two end-member age evolutions (Fig. 7). The red path describes the most likely age evolution given the quality of the results within individual samples. The solution implies that the Adrar-n-Takoucht Formation was emplaced from 575 to 570 Ma, followed very quickly by the emplacement of the Tadoughast Formation around 569 Ma. According to this path, severe Pb loss affected samples OU72B, OU75 and OU63, with more than half of their dataset reflecting this effect. This path is considered the most robust as it is supported by the two best results coming from samples OU72B and OU87. This path constrains the time gaps between the emplacement of the formations to less than 1 Myr. An alternative age path, which would lead to a maximum time gap between the ages of poles B1 and C, corresponds to the yellow path (Fig. 7). The path ignores the data from OU71A that yielded an age 4 Myrs younger than sample OU72B located in the same magmatic sequence, which are thus expected to have a similar age. In addition, samples OU13 and OU63 share common ages and are given more weight in this alternative path than the age given by OU87, despite the high quality of its determination.

To estimate the rate of paleomagnetic directional variations between the time of acquisition of poles B1 and C, we employed a Monte Carlo approach, which allows to take into account both the age and spatial uncertainties of each pole. For each pole, we drew 100,000 simulated ages from a Gaussian age distribution based on our geochronologic results, and 100,000 simulations of the pole drawn from a Fisher distribution based on the properties of the pole (Table 2). With these 100,000 simulated age-pole pairs from each of the two poles, we then computed 100,000 rates of change (Fig. 8a and b). This procedure was followed twice in order to estimate the median and associated 95% confidence bounds for the red and yellow paths shown in Fig. 7. For the red path, the ages of poles B1 and C are defined by samples

Table 2. Statistical parameters for calculating rates of change

Pole	Latitude (°)	Longitude (°)	A_{95}	K	Mean Age^{red} (Ma)	2σ	Mean Age^{yellow} (Ma)	2σ
B1	21,9	31	15,6	5,3	569,2	0,6	565,7	1,3
C	-57,6	295,6	15,7	11,7	571,1	1,1	575,0	0,8

Path	Rates* (°/Myrs)	[0.025, 0.975]**
Red	56,8	[23.4, 171.1]
Yellow	11,6	[5.5, 17.9]

*Median value, **Value of the 2.5th and 97.5th centiles

OU87 and OU71A respectively, yielding a median speed of 56.8°/Myr with 95% confidence bounds of 23.4°/Myr and 171.1°/Myr. For the yellow path, the ages of components B1 and C are defined by the younger solution of sample OU63 and sample OU72B, respectively, yielding a median speed of 11.6°/Myr with 95% confidence bounds of 5.5°/Myr and 17.9°/Myr.

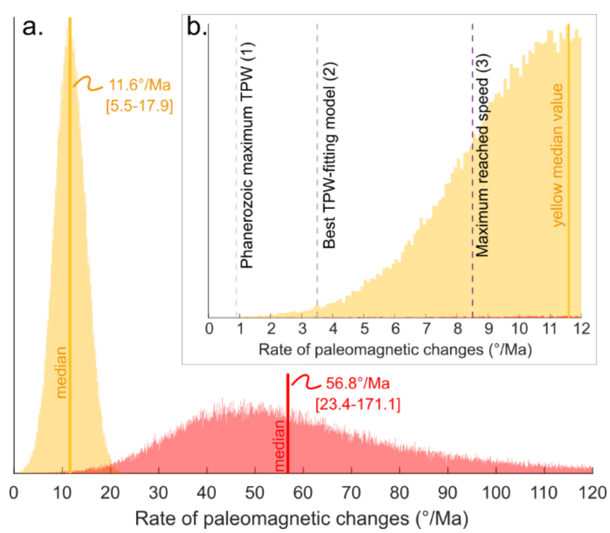

Figure 8: *a. Histogram of the rates of change computed with a Monte Carlo method using the age distributions defined by the yellow and red paths (Table 2). Numbers in square brackets are the 95% confidence bounds of each rate distribution. b. Same histogram as in (a), but zoomed-in to the rate range of 0-12°/Ma. References: (1) Torsvik et al. (2014), (2) Robert et al. (2018), (3) Creveling et al. (2012).*

5.4. Test of the True Polar Wander hypothesis

The speed limit of TPW results from the competition between the amplitude of inertial perturbations associated with changes to the distribution of mass heterogeneities, and mantle viscosity that controls how fast mass is redistributed in the mantle. During a TPW episode, the instantaneous rate at which the pole moves is not constant but grows up to a transient maximum value before decreasing again, and is therefore distinct from the rate of change integrated over the entire TPW event. Because the paleomagnetic data for the Ediacaran are sparse and only display two groups of poles separated by about 111 ± 31° (Fig. 1), the paleomagnetic rates of change are comparable with the integrated rate but not with the maximum TPW (usually reported in publications), the latter being an overestimation of the former.

In the following, we review numerical estimates of TPW speed from the literature to compare with our APWP rate of change. Note that when the integrated rate was not available, we reported the maximum rate. Steinberger and O'Connell (2002) estimated a maximum TPW rate of about 1°/Myrs using models of mantle mass heterogeneities built with tomographic images and flow field simulations of the Cenozoic. Tsai and Stevenson (2007) determined a maximum rate of 2.4°/Myrs by prescribing rapid and oscillating perturbations to the non-hydrostatic moments of inertia. This is consistent with the TPW speed estimated from paleomagnetic data over the last 550 Ma that is around 1-2°/Myrs (Besse and Courtillot, 2002; Evans, 2003; Torsvik et al., 2014). However, our new rate estimates are much higher than these estimated speed limits (Fig. 8b). Tsai and Stevenson (2007) pointed out that much faster TPW (88° in 10 Myrs) could be reached if the mantle viscosity was much lower ($\eta = 10^{21}$ Pa.s), which they considered unreasonably low. Fu et al. (2022) proposed that mantle viscosity in the mid-Neoproterozoic was lower, allowing for faster TPW, both because of hotter mantle conditions in the Precambrian and heat accumulated during the lifetime of the supercontinent Rodinia. However, this scenario remains to be tested with numerical simulations for assessing a maximum TPW rate.

Faster TPW can also be reached in the case of major changes in the distribution of mantle mass heterogeneities. Rose et al. (2017) argued that faster TPW could occur in the case where inertial perturbations were sufficiently high to produce a large offset between the maximum axis of inertia and the spin axis. They estimated a maximum rate of change of ~6°/Myrs during such a TPW event based on a scaling analysis of TPW. Robert et al. (2018) found that a cessation in global subduction for ~90 Myrs followed by a restart of a girdle of subduction surrounding the continents at the beginning of the Ediacaran could produce a similarly fast episode of TPW, fitting, to first order, the amplitude of polar wander defined by the paleomagnetic data. They obtained a maximum rate of ~6.5°/Myrs and an integrated rate of 3.2°/Myrs. These rates are much lower than the range obtained in this study (Fig. 8b), and even the slowest estimate of 11.6°/Myrs significantly exceeds them. Creveling et al. (2012) simulated TPW episodes of up to 51° in 6 Myrs (integrated rate of ~8.5°/Myrs) in the case where the geometry of mantle flow imposes a strong prolate shape in the Earth's figure. Such a rate overlaps with the uncertainty range associated with the 'yellow' models. However, the oscillatory mechanism that they propose can only account for up to 45-50° in TPW amplitude, and cannot explain the 111 ± 31° defined by the paleomagnetic data. In any case, none of the modelled estimates can explain the rates calculated for the faster alternative (red path), which we consider more robust on the basis of our analysis of the geochronological data. The hypothesis of TPW is therefore difficult to reconcile with the new data presented in this study.

5.5. An alternative solution: the equatorial dipole field hypothesis

The alternative hypotheses to TPW comprise the presence of remagnetization, ultra-fast plate motion and geomagnetic field perturbations. Because our poles are both supported by positive field tests, we consider the hypothesis of remagnetization unlikely. Like TPW, differential plate motion is also speed-limited by mantle viscosity to some 20-30 cm/yr (Domeier et al., 2023), so ultra-fast plate motion alone is difficult to reconcile with our rate estimates. Regarding the hypothesis of magnetic field perturbations, two models of the geomagnetic field have been proposed to explain the observational paleomagnetic record. (1) Abrajevitch and Van der Voo (2010) proposed that the Ediacaran geomagnetic field significantly departed from a geocentric axial dipole field. They hypothesized that the field was dominated by a magnetic dipole oscillating between an axial and equatorial alignment, based on the geodynamo simulations of Ishihara and Kida (2000, 2002) and Aubert and Wicht (2004). Alternatively, (2) Halls et al. (2015) suggested that the appearance of an equatorial dipole could be intimately linked to reversals of the axial dipole, following the numerical experiments of Gissinger et al. (2012). In the model of Halls et al. (2015), the magnetic field was of very low intensity and was reversing very frequently, allowing the paleomagnetic record to capture an equatorial dipole as a transitional field. Both models would allow rates of directional change as high as those occurring during a magnetic reversal--of the order of several degrees per Kyr--and are therefore compatible with our rate estimates.

The model of Halls et al. (2015) can be directly tested using paleomagnetic observations such as reversal frequency and paleointensity. Robert et al. (2017) reported few reversals associated with components B1 and C, but the continuity of the paleofield record provided by the corresponding volcanic rocks is unknown, so it is not possible to make an estimate of the reversal frequency. However, a coeval paleomagnetic study conducted on ~574 Ma sedimentary rocks from the Johnnie Formation in Laurentia yielded an estimate of 13 reversals per Myr (Kodama, 2021), suggesting a high reversal rate during the acquisition of components B1 and C. Paleointensity estimates reported in the literature from around 570 Ma also suggest a peculiar magnetic field behavior. Bono et al. (2019) reported a paleointensity about ten times lower than that of Earth's present-day field from a study of the 565 ± 4 Ma Sept-Iles intrusion in Laurentia. A similarly low paleointensity estimate has also been reported from the 561-580 Ma Ratne volcanic suite in Baltica by Shcherbakova et al. (2020) and Thallner et al. (2022). Collectively, these data support the notion that the field was extremely weak and reversing very frequently around 570 Ma, which could have enhanced the record of transitional directions. However, the B1 and C poles are derived from dual-polarity directions, which are likely to represent a dominantly dipole field rather than chaotic transitional directions. The arc distance of 111 ± 31° between poles B1 and C is in agreement with the occurrence of an equatorial dipole field. Nevertheless, our components are observed sequentially and not mixed along the stratigraphy, which suggests the appearance of a relatively stable equatorial dipole, in favor of the model of Abrajevitch and Van der Voo (2010), rather than a short-lived and transitional one as would be expected in the scenario of Halls et al. (2015).

The occurrence of an equatorial dipole field in the Ediacaran would have significant implications for paleogeographic reconstructions. If the equatorial dipole field was approximately pinned in longitude, poles produced by the axial and equatorial dipole fields from several continents could be adjusted to produce longitudinally-constrained paleogeographic reconstructions. The adjustment of the rapid shifts in Ediacaran APWPs has already been attempted by Robert et al. (2017, 2018, 2021) and Wen et al. (2020, 2022). The solution by Robert et al. (2021) is shown in Figure 9a, where the selected paleomagnetic poles (filled symbols) are separated into two groups of poles ~90° apart, consistent with a magnetic field switching from an axial to an equatorial alignment. Because of the ~90° arc distance between these groups (Table 3), there is an ambiguity about the polarity of their constituent poles, yielding non-unique paleogeographic solutions. However, the fit of Robert et al. (2021) produces a geologically- and kinematically-consistent paleogeographic reconstruction in agreement with younger reconstructions from the Cambrian (e.g. Torsvik et al. 2014). We note that the recently published pole JO (Johnnie Formation; Kodama, 2021) lies off the path connecting the axial and equatorial dipole field. This pole, being associated with a negative reversal test, might be contaminated by a secondary magnetization or may indicate a more complex magnetic field behavior. Regarding poles RV (Rafalovka volcanics; Shcherbakova et al., 2020) and AF (Avellaneda Formation; Franceschinis et al., 2022), they fall in between the axial and equatorial dipole positions depicted in Figure 9a and may represent intermediate dipole states, or in the case of pole AF, a minor adjustment of the position of Rio de la Plata relative to the other Gondwana blocks could improve its fit to the surrounding poles.

Table 3. Paleomagnetic poles between 560-580 Ma

ID	Geologic unit	Lat (°)	Lon (°)	A_{95} (°)	References	Age (Ma)	Method	Age reference
West Africa								
B1	Fajjoud-Tadoughast volcanics	21.9	31	15.6	Robert et al. (2017)	569.2 ± 0.6	CA-ID-TIMS (U-Pb)	*This study*
C	Adrar-n-Takoucht volcanics	-57.6	295.6	15.7	Robert et al. (2017)	571.1 ± 1.1	CA-ID-TIMS (U-Pb)	*This study*
Rio de la Plata								
LB	Los Barrientos claystones	-15.1	252.6	12.4*	Rapalini (2006)	570	APWP	Rapalini et al. (2015)
AF	Avellaneda formation	-1	313.4	5.9	Franceschinis et al. (2022)	570	Strat. & carb. Iso.	Franceschinis et al. (2022)
SA	Sierra de las Animas volcanics	-12.2	258.9	14.9	Rapalini et al. (2015)	578 ± 4	SHRIMP (U-Pb)	Rapalini et al. (2015)
Congo-Sao Francisco								
NO	Nola dolerite dykes	-61.8	304.8	7.6	Moloto-A-Kenguemba et al. (2008)	571 ± 6	$^{40}Ar/^{39}Ar$	Moloto-A-Kenguemba et al. (2008)
Laurentia								
SIA	Sept-Iles intrusion, comp. A	141	20	6.7^{*x}	Tanczyk et al. (1987)	565 ± 4	U-Pb	Higgins and von Breemen (1998)
SIB	Sept-Iles intrusion, comp. B	116	-59	10.0^{*x}	Tanczyk et al. (1987)	565 ± 4	U-Pb	Higgins and von Breemen (1998)
SI**	Sept-Iles intrusion, single-cryst.	346	-4.3	10.8	Bono and Tarduno (2015)	565 ± 4	U-Pb	Higgins and von Breemen (1998)
JF	Johnnie formation	348.4	11.7	8.6	Kodama (2021)	574	carbon isotope	Rooney et al. (2020)
CTA	Catoctin volcanics, comp. A	42	296.7	17.5^{*x}	Meert et al. (1994)	572 ± 5	U-Pb	Aleinikoff et al. (1995)
CTB	Catoctin volcanics, comp. B	4	3	9.5^{*x}	Meert et al. (1994)	572 ± 5	U-Pb	Aleinikoff et al. (1995)
CC	Callander Complex	46.3	301.4	6	Symons and Chiasson (1991)	577 ± 1	U-Pb	Kamo et al. (1995)
Baltica								
BA	Basu formation	-2	6	3.8	Levashova et al. (2015)	565 ± 5	Stratigraphy	see in Levashova et al. (2015)
KF	Kurgashlya formation	50.9	314.5	5.3	Lubnina et al. (2014)	600-570	Stratigraphy	Puchkov, 2012
BK	Bakeevo formation	42.3	299.1	5.3	Lubnina et al. (2014)	600-570	Stratigraphy	Puchkov, 2012
RV	Rafalovka volcanics	44.8	342	9.2	Shcherbakova et al. (2020)	580 ± 9	$^{40}Ar/^{39}Ar$	Elming et al. (2007)

^{x}calculated in McCausland et al. (2007)

*recalculated using dp and dm.

**pole calculated for a site location of lat=50.15°N, lon=293.6°E by combining components A and B of Bono and Tarduno (2015)

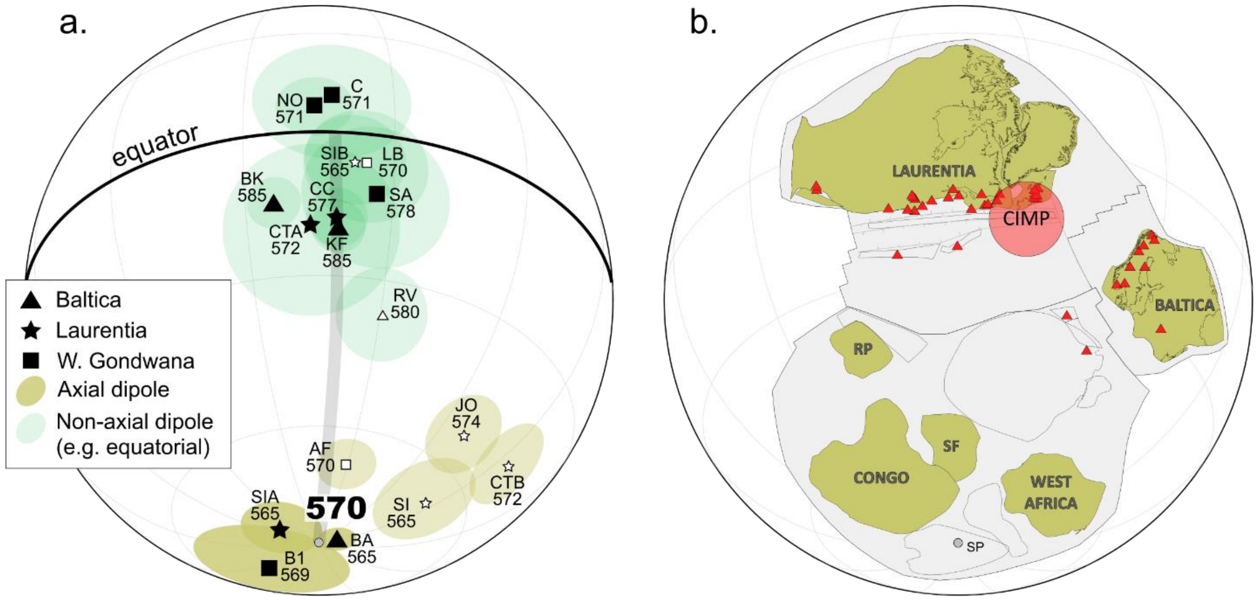

Figure 9: a. Distribution of the 560-580 Ma paleomagnetic poles from West Gondwana, Laurentia and Baltica listed in Table 3. Poles are rotated using the rotation parameters of Robert et al. (2021) at 565 Ma. Filled (open) symbols represent poles used (unused) in the reconstruction of Robert et al. (2021). The grey path illustrates the departure of the dipole from its axial to equatorial position. b. Corresponding paleogeographic reconstruction where the position of West Gondwana, Laurentia and Baltica are longitudinally adjusted (see text). The inferred emplacement center of the Central Iapetus Magmatic Province (CIMP) and the associated relics (triangles) are displayed in red following Robert et al. (2021). Abbreviations: RP=Rio de la Plata, SF=Sao Francisco, SP=South pole.

If the field was flipping from an axial to an equatorial dipole state, which group would correspond to which state? If pole B1 and the poles surrounding it in Figure 9a represented the axial dipole state, West Africa, Baltica and Laurentia would have lain at high, mid and low latitudes respectively at around 570 Ma (Figure 9b), whereas the alternative possibility (as defined by pole C and the poles surrounding it in Figure 9a) would have yielded a low latitude for West Africa, and a high latitude for Laurentia. The predicted paleolatitudes in the former case are similar to those for the same blocks in plate reconstructions of the Cambrian (e.g. Torsvik et al., 2014), which imply that this field state assignment requires smaller plate motions than the alternative state. Interestingly, because West Africa would have remained at high latitudes if reconstructed with pole B1, it would have potentially experienced cold climatic conditions. Glacially-derived rocks dated between 592 and 579 Ma have been identified in Morocco (Letsch et al., 2018; Youbi et al. 2020) and could support a high latitude for West Africa. However, this inference remains speculative at this stage; a more thorough analysis of the latitudinal distribution of glacial deposits of the surrounding blocks as reconstructed with paleomagnetic data assuming these alternative field states could be illuminating. Another appealing aspect of assigning pole B1 as the axial dipole is related to the corresponding position of the equatorial dipole (as defined by pole C and the poles surrounding it in Figure 9a). Abrajevitch and Van der Voo (2010) speculated that the position of the equatorial dipole field could be controlled by heat flux heterogeneities at the core-mantle boundary, and notably by an Ediacaran plume under Laurentia, interpreted as responsible for the emplacement of the Central Iapetus Magmatic Province (Puffer, 2002; Tegner et al., 2019). Our paleogeographic reconstruction (Figure 9b) is in agreement with this inference, which may suggest that the mantle played an important role in controlling the geometry of the Ediacaran geomagnetic field.

6. Conclusions

This paper addresses the possibility of rapid true polar wander during the Ediacaran by presenting new geochronological constraints on the apparent polar wander of West Africa. Using the CA ID TIMS method on zircons, we dated seven samples that are stratigraphically distributed across a stratigraphic section recording a large apparent polar wander shift of mid-Ediacaran age. The samples display significant dispersion in the measured dates due to both Pb loss and the presence of antecrysts and xenocrysts. Despite these limitations, several samples yielded age plateaus that we interpret as the age of emplacement of the pyroclastic rocks. We tested two end-member age progressions, a fast evolution relying on the samples yielding the most robust data, and a slow evolution that includes less robust data but which maximizes the time allowed for the observed apparent polar wander. To account for the spatial and temporal uncertainties associated with both the paleomagnetic poles and the geochronological constraints, we adopted a Monte Carlo approach. Using this method, we estimated rates of change of 11.6°/Myrs [5.5 – 17.9] for the slow option and 56.8°/Myrs [23.4 – 171.1] for the fast option. These rates are too high to be explained by true polar wander. Instead, they can be better explained as perturbations of the magnetic field during the Ediacaran and notably by an unstable magnetic field flipping from an axial to an equatorial dipole position.

Acknowledgments

We thank Augusto Rapalini, an anonymous reviewer, and the associate editor Sergei Pisarevsky for their constructive reviews. This work was supported by the Research Council of Norway (RCN) project 250111, through RCN's Centres of Excellence funding scheme, project 223272 (CEED), and from the European Research Council (ERC) under the European Union's Horizon 2020 research and innovation program (Grant agreement No. 101043844).

References

Abrajevitch, A., & Van der Voo, R. (2010). Incompatible Ediacaran paleomagnetic directions suggest an equatorial geomagnetic dipole hypothesis. Earth and Planetary Science Letters, 293(1-2), 164-170.

Aleinikoff, J. N., Zartman, R. E., Walters, M., Rankin, D. W., Lyttle, P. T., & Burton, W. C. (1995). U-Pb ages of metarhyolites of the Catoctin and Mount Rogers Formations, central and southern Appalachians: Evidence for two pulses of Iapetan rifting. American Journal of Science, 295(4), 428-454.

Aubert, J., & Wicht, J. (2004). Axial vs. equatorial dipolar dynamo models with implications for planetary magnetic fields. Earth and Planetary Science Letters, 221(1-4), 409-419.

Bazhenov, M. L., Levashova, N. M., Meert, J. G., Golovanova, I. V., Danukalov, K. N., & Fedorova, N. M. (2016). Late Ediacaran magnetostratigraphy of Baltica: evidence for magnetic field hyperactivity?. Earth and Planetary Science Letters, 435, 124-135.

Benziane, F. (2007). Lithostratigraphie et évolution géodynamique de l'Anti-Atlas (Maroc) du paléoprotérozoïque au néoprotérozoïque: exemples de la boutonnière de Tagragra Tata et du Jebel Saghro (Doctoral dissertation, Chambéry).

Besse, J., & Courtillot, V. (2002). Apparent and true polar wander and the geometry of the geomagnetic field over the last 200 Myr. Journal of Geophysical Research: Solid Earth, 107(B11), EPM-6.

Blein, O., Baudin, T., Chevremont, P., Soulaimani, A., Admou, H., Gasquet, P., ... & Gombert, P. (2014a). Geochronological constraints on the polycyclic magmatism in the Bou Azzer-El Graara inlier (central Anti-Atlas Morocco). Journal of African Earth Sciences, 99, 287-306.

Blein, O., Baudin, T., Soulaimani, A., Cocherie, A., Chèvremont, P., Admou, H., ... & Roger, J. (2014b). New geochemical, geochronological and structural constraints on the Ediacaran evolution of the south Sirwa, Agadir-Melloul and Iguerda inliers, Anti-Atlas, Morocco. Journal of African Earth Sciences, 98, 47-71.

Bonhomme, M., Hassenforder, B. .Le. (1985). Métamorphisme hercynien dans les formations tardi et post-panafricaines de l'Anti-Atlas occidental (Maroc). Données isotopiques Rb/Sr et K/Ar des fractions fines. Sci. Géol. Bull. (38), 175–183

Bono, R. K., & Tarduno, J. A. (2015). A stable Ediacaran Earth recorded by single silicate crystals of the ca. 565 Ma Sept-Îles intrusion. Geology, 43(2), 131-134.

Bono, R. K., Tarduno, J. A., Nimmo, F., & Cottrell, R. D. (2019). Young inner core inferred from Ediacaran ultra-low geomagnetic field intensity. Nature Geoscience, 12(2), 143-147.

Boudzoumou, F., Vandamme, D., Affaton, P., Gattacceca, J., Ouazzani, H., Badra, L., & Mahjoubi, E. (2012). Evidence of a Permian remagnetization in the Neoproterozoic-Cambrian Adoudounian Formation (Anti-Atlas, Morocco). Bulletin de l'Institut Scientifique, Rabat, section Sciences de la Terre, 34, 15-28.

Charlot, R. (1976). The Precambrian of the Anti-Atlas (Morocco): a geochronological synthesis. Precambr. Res. 3 (3), 273–299.

Corfu, F. (2004). U–Pb age, setting and tectonic significance of the anorthosite–mangerite–charnockite–granite suite, Lofoten–Vesterålen, Norway. Journal of Petrology, 45(9), 1799-1819.

Creveling, J. R., Mitrovica, J. X., Chan, N. H., Latychev, K., & Matsuyama, I. (2012). Mechanisms for oscillatory true polar wander. Nature, 491(7423), 244-248.

De Silva, S. L., Riggs, N. R., & Barth, A. P. (2015). Quickening the pulse: Fractal tempos in continental arc magmatism. Elements, 11(2), 113-118.

Domeier, M., Robert, B., Meert, J. G., Kulakov, E. V., McCausland, P. J., Trindade, R. I., & Torsvik, T. H. (2023). The enduring Ediacaran paleomagnetic enigma. Earth-Science Reviews, 104444.

Driscoll, P. E. (2016). Simulating 2 Ga of geodynamo history. Geophysical Research Letters, 43(11), 5680-5687.

Elming, S. A., Kravchenko, S. N., Layer, P., Rusakov, O. M., Glevasskaya, A. M., Mikhailova, N. P., & Bachtadse, V. (2007). Palaeomagnetism and 40Ar/39Ar age determinations of the Ediacaran traps from the southwestern margin of the East European Craton, Ukraine: relevance to the Rodinia break-up. Journal of the Geological Society, 164(5), 969-982.

Evans, D. A. (1998). True polar wander, a supercontinental legacy. Earth and Planetary Science Letters, 157(1-2), 1-8.

Evans, D. A. (2003). True polar wander and supercontinents. Tectonophysics, 362(1-4), 303-320.

Franceschinis, P. R., Afonso, J. W., Arrouy, M. J., Gómez-Peral, L. E., Poiré, D., Trindade, R. I. F., & Rapalini, A. E. (2022). Paleomagnetism of the Ediacaran Avellaneda Formation (Argentina), part I: Paleogeography of the Río de la Plata craton at the dawn of Gondwana. Precambrian Research, 383, 106909.

Fu, H., Zhang, S., Condon, D. J., & Xian, H. (2022). Secular change of true polar wander over the past billion years. Science Advances, 8(41), eabo2753.

Gasquet, D., Ennih, N., Liégeois, J. P., Soulaimani, A., & Michard, A. (2008). The pan-african belt. In Continental evolution: the geology of Morocco (pp. 33-64). Springer, Berlin, Heidelberg.

Gissinger, C., Petitdemange, L., Schrinner, M., & Dormy, E. (2012). Bistability between equatorial and axial dipoles during magnetic field reversals. Physical review letters, 108(23), 234501.

Grazhdankin, D. V., Marusin, V. V., Meert, J., Krupenin, M. T., & Maslov, A. V. (2011, September). Kotlin regional stage in the South Urals. In Doklady Earth Sciences (Vol. 440, No. 1, p. 1222). Springer Nature BV.

Halls, H. C., Lovette, A., Hamilton, M., & Söderlund, U. (2015). A paleomagnetic and U–Pb geochronology study of the western end of the Grenville dyke swarm: Rapid changes in paleomagnetic field direction at ca. 585 Ma related to polarity reversals?. Precambrian Research, 257, 137-166.

Higgins, M. D., & Breemen, O. V. (1998). The age of the Sept Iles layered mafic intrusion, Canada: implications for the late Neoproterozoic/Cambrian history of southeastern Canada. The Journal of Geology, 106(4), 421-432.

Hodych, J. P., Cox, R. A., & Košler, J. (2004). An equatorial Laurentia at 550 Ma confirmed by Grenvillian inherited zircons dated by LAM ICP-MS in the Skinner Cove volcanics of western Newfoundland: implications for inertial interchange true polar wander. Precambrian Research, 129(1-2), 93-113.

Hollard, H., Choubert, G., Bronner, G., Marchand, J., Sougy, J. (1985). Carte géologique du Maroc, échelle: 1/1.000.000. Notes Mém. Serv. Géol. Maroc, no 260.

Ishihara, N., & Kida, S. (2000). Axial and equatorial magnetic dipoles generated in a rotating spherical shell. Journal of the Physical Society of Japan, 69(6), 1582-1585.

Ishihara, N., & Kida, S. (2002). Equatorial magnetic dipole field intensification by convection vortices in a rotating spherical shell. Fluid dynamics research, 31(4), 253.

Jaffey, A. H., Flynn, K. F., Glendenin, L. E., Bentley, W. T., & Essling, A. M. (1971). Precision measurement of half-lives and specific activities of U 235 and U 238. Physical review C, 4(5), 1889.

Kamo, S. L., Krogh, T. E., & Kumarapeli, P. S. (1995). Age of the Grenville dyke swarm, Ontario–Quebec: implications for the timing of Iapetan rifting. Canadian Journal of Earth Sciences, 32(3), 273-280.

Ketcham, R. A., Donelick, R. A., & Carlson, W. D. (1999). Variability of apatite fission-track annealing kinetics: III. Extrapolation to geological time scales. American Mineralogist, 84(9), 1235-1255.

Kirschvink, J. L., Ripperdan, R. L., & Evans, D. A. (1997). Evidence for a large-scale reorganization of Early Cambrian continental masses by inertial interchange true polar wander. Science, 277(5325), 541-545.

Kodama, K. P. (2021). Combined Magnetostratigraphy From Three Localities of the Rainstorm Member of the Johnnie Formation in California and Nevada, United States Calibrated by Cyclostratigraphy: A 13 R/Ma Reversal Frequency for the Ediacaran. Frontiers in Earth Science, 1086.

Krogh, T. (1973). A low-contamination method for hydrothermal decomposition of zircon and extraction of U and Pb for isotopic age determinations. Geochimica et Cosmochimica Acta, 37(3), 485-494.

Levashova, N. M., Golovanova, I. V., Rudko, D. V., Danukalov, K. N., Rudko, S. V., Salmanova, R. Y., & Meert, J. G. (2021). Late Ediacaran magnetic field hyperactivity: Quantifying the reversal frequency in the Zigan Formation, Southern Urals, Russia. Gondwana Research, 94, 133-142.

Letsch, D., Large, S. J., Buechi, M. W., Winkler, W., & von Quadt, A. (2018). Ediacaran glaciations of the West African Craton–evidence from Morocco. Precambrian research, 310, 17-38.

Levashova, N. M., Bazhenov, M. L., Meert, J. G., Danukalov, K. N., Golovanova, I. V., Kuznetsov, N. B., & Fedorova, N. M. (2015). Paleomagnetism of upper Ediacaran clastics from the South Urals: Implications to paleogeography of Baltica and the opening of the Iapetus Ocean. Gondwana Research, 28(1), 191-208.

Li, Z. X., Bogdanova, S., Collins, A. S., Davidson, A., De Waele, B., Ernst, R. E., ... & Vernikovsky, V. (2008). Assembly, configuration, and break-up history of Rodinia: a synthesis. Precambrian research, 160(1-2), 179-210.

Lubnina, N. V., Pisarevsky, S. A., Puchkov, V. N., Kozlov, V. I., & Sergeeva, N. D. (2014). New paleomagnetic data from Late Neoproterozoic sedimentary successions in Southern Urals, Russia: implications for the Late Neoproterozoic paleogeography of the Iapetan realm. International Journal of Earth Sciences, 103, 1317-1334.

Ludwig, K.R. (2009). Isoplot 4.1. A geochronological toolkit for microsoft excel. 4. Berkeley Geochronology Center Spec. Publ., pp. 76

Mattinson, J. M. (2005). Zircon U–Pb chemical abrasion (“CA-TIMS”) method: combined annealing and multi-step partial dissolution analysis for improved precision and accuracy of zircon ages. Chemical Geology, 220(1-2), 47-66.

Maslov, A. V., Meert, J., Levashova, N. M., Ronkin, Y. L., Grazhdankin, D. V., Kuznetsov, N. B., ... & Ipat'eva, I. S. (2013, March). New constraints for the age of Vendian glacial deposits (Central Urals). In Doklady earth sciences (Vol. 449, No. 1, p. 303). Springer Nature BV.

McCausland, P. J., Van der Voo, R., & Hall, C. M. (2007). Circum-Iapetus paleogeography of the Precambrian–Cambrian transition with a new paleomagnetic constraint from Laurentia. Precambrian Research, 156(3-4), 125-152.

Meert, J. G., Van der Voo, R., & Payne, T. W. (1994). Paleomagnetism of the Catoctin volcanic province: A new Vendian-Cambrian apparent polar wander path for North America. Journal of Geophysical Research: Solid Earth, 99(B3), 4625-4641.

Miller, J. S., Matzel, J. E., Miller, C. F., Burgess, S. D., & Miller, R. B. (2007). Zircon growth and recycling during the assembly of large, composite arc plutons. Journal of Volcanology and Geothermal Research, 167(1-4), 282-299.

Moloto-A-Kenguemba, G. R., Trindade, R. I., Monié, P., Nédélec, A., & Siqueira, R. (2008). A late Neoproterozoic paleomagnetic pole for the Congo craton: Tectonic setting, paleomagnetism and geochronology of the Nola dike swarm (Central African Republic). Precambrian Research, 164(3-4), 214-226.

Puchkov, V. N. (2012, November). On the age of the Asha series, South Urals. In Geology, Mineral Resources, and Geoecological Problems of Bashkortostan, Ural, and Adjacent Areas: Proceedings of the IX Interregional Science-and-Practice Conference, Ufa, Russia (pp. 47-51).

Puffer, J. H. (2002). A late Neoproterozoic eastern Laurentian superplume: Location, size, chemical composition, and environmental impact. American Journal of Science, 302(1), 1-27.

Rapalini, A. E. (2006). New Late Proterozoic paleomagnetic pole for the Rio de la Plata craton: implications for Gondwana. Precambrian Research, 147(3-4), 223-233.

Rapalini, A. E., Tohver, E., Bettucci, L. S., Lossada, A. C., Barcelona, H., & Pérez, C. (2015). The late Neoproterozoic Sierra de las Ánimas Magmatic Complex and Playa Hermosa Formation, southern Uruguay, revisited: Paleogeographic implications of new paleomagnetic and precise geochronologic data. Precambrian Research, 259, 143-155.

Robert, B., Besse, J., Blein, O., Greff-Lefftz, M., Baudin, T., Lopes, F., ... & Belbadaoui, M. (2017). Constraints on the Ediacaran inertial interchange true polar wander hypothesis: A new paleomagnetic study in Morocco (West African Craton). Precambrian Research, 295, 90-116.

Robert, B., Greff-Lefftz, M., & Besse, J. (2018). True polar wander: A key indicator for plate configuration and mantle convection during the late Neoproterozoic. Geochemistry, Geophysics, Geosystems, 19(9), 3478-3495.

Ronkin, Y. L., Grazhdankin, D. V., Maslov, A. V., Mizens, G. A., Matukov, D. I., Krupenin, M. T., ... & Kornilova, A. Y. (2006, November). U-Pb (SHRIMP II) age of zircons from ash beds of the chernokamen formation, Vendian Sylvitsa group (Central Urals). In Doklady earth sciences (Vol. 411, No. 2, p. 1341). Springer Nature BV.

Rooney, A. D., Cantine, M. D., Bergmann, K. D., Gómez-Pérez, I., Al Baloushi, B., Boag, T. H., ... & Strauss, J. V. (2020). Calibrating the coevolution of Ediacaran life and environment. Proceedings of the National Academy of Sciences, 117(29), 16824-16830.

Rose, I., & Buffett, B. (2017). Scaling rates of true polar wander in convecting planets and moons. Physics of the Earth and Planetary Interiors, 273, 1-10.

Schoene, B. (2014). 4.10-u–th–pb geochronology. Treatise on geochemistry, 4, 341-378.

Sebti, S., Saddiqi, O., El Haimer, F.Z., Michard, A., Ruiz, G., Bousquet, R., Baidder, L., de Lamotte, D.F., 2009. Vertical movements at the fringe of the West African Craton: first zircon fission track datings from the Anti-Atlas Precambrian basement, Morocco. C.R. Geosci. 341 (1), 71–77.

Shcherbakova, V. V., Bakhmutov, V. G., Thallner, D., Shcherbakov, V. P., Zhidkov, G. V., & Biggin, A. J. (2020). Ultra-low palaeointensities from East European Craton, Ukraine support a globally anomalous palaeomagnetic field in the Ediacaran. Geophysical Journal International, 220(3), 1928-1946.

Souleimani, A., Egal, E., Razin, P., Youbi, N., Admou, H., Blein, O., Barbanson, L., Gasquet, D., Bouabdelli, M. and Anzar, C. Notice explicative carte géologique Maroc (1/50 000), feuille Agadir Melloul, Notes et Mémoires Services Géologiques du Maroc (:549), 2013, pp. carte.

Soulaimani, A., Ouanaimi, H., Saddiqi, O., Baidder, L., & Michard, A. (2018). The anti-atlas pan-african belt (Morocco): overview and pending questions. Comptes Rendus Geoscience, 350(6), 279-288.

Stacey, J. T., & Kramers, 1. (1975). Approximation of terrestrial lead isotope evolution by a two-stage model. Earth and planetary science letters, 26(2), 207-221.

Steinberger, B., & O'Connell, R. J. (2002). The convective mantle flow signal in rates of true polar wander. Ice Sheets, Sea Level and the Dynamic Earth, Geodyn. Ser, 29, 233-256.

Symons, D. T. A., & Chiasson, A. D. (1991). Paleomagnetism of the Callander Complex and the Cambrian apparent polar wander path for North America. Canadian Journal of Earth Sciences, 28(3), 355-363.

Tanczyk, E. I., Lapointe, P., Morris, W. A., & Schmidt, P. W. (1987). A paleomagnetic study of the layered mafic intrusion at Sept-Iles, Quebec. Canadian Journal of Earth Sciences, 24(7), 1431-1438.

Tegner, C., Andersen, T. B., Kjøll, H. J., Brown, E. L., Hagen-Peter, G., Corfu, F., ... & Torsvik, T. H. (2019). A mantle plume origin for the Scandinavian dyke complex: A "piercing point" for 615 Ma plate reconstruction of Baltica?. Geochemistry, Geophysics, Geosystems, 20(2), 1075-1094.

Thallner, D., Biggin, A. J., & Halls, H. C. (2021). An extended period of extremely weak geomagnetic field suggested by palaeointensities from the Ediacaran Grenville dykes (SE Canada). Earth and Planetary Science Letters, 568, 117025.

Thallner, D., Shcherbakova, V. V., Bakhmutov, V. G., Shcherbakov, V. P., Zhidkov, G. V., Poliachenko, I. B., & Biggin, A. J. (2022). New palaeodirections and palaeointensity data from extensive profiles through the Ediacaran section of the Volyn Basalt Province (NW Ukraine). Geophysical Journal International, 231(1), 474-492.

Thomas, R. J., Chevallier, L. P., Gresse, P. G., Harmer, R. E., Eglington, B. M., Armstrong, R. A., ... & Ingram, B. A. (2002). Precambrian evolution of the Sirwa window, Anti-Atlas orogen, Morocco. Precambrian Research, 118(1-2), 1-57.

Thomas, R. J., Fekkak, A., Ennih, N., Errami, E., Loughlin, S. C., Gresse, P. G., ... & Liégeois, J. P. (2004). A new lithostratigraphic framework for the Anti-Atlas Orogen, Morocco. Journal of African Earth Sciences, 39(3-5), 217-226.

Torsvik, T. H., van der Voo, R., Doubrovine, P. V., Burke, K., Steinberger, B., Ashwal, L. D., ... & Bull, A. L. (2014). Deep mantle structure as a reference frame for movements in and on the Earth. Proceedings of the National Academy of Sciences, 111(24), 8735-8740.

Tsai, V. C., & Stevenson, D. J. (2007). Theoretical constraints on true polar wander. Journal of Geophysical Research: Solid Earth, 112(B5).

Villeneuve, M., & Cornée, J. J. (1994). Structure, evolution and palaeogeography of the West African craton and bordering belts during the Neoproterozoic. Precambrian Research, 69(1-4), 307-326.

Walsh, G. J., Aleinikoff, J. N., Benziane, F., Yazidi, A., & Armstrong, T. R. (2002). U–Pb zircon geochronology of the Paleoproterozoic Tagragra de Tata inlier and its Neoproterozoic cover, western Anti-Atlas, Morocco. Precambrian Research, 117(1-2), 1-20.

Wen, B., Evans, D. A., Anderson, R. P., & McCausland, P. J. (2020). Late Ediacaran paleogeography of Avalonia and the Cambrian assembly of West Gondwana. Earth and Planetary Science Letters, 552, 116591.

Wen, B., Luo, C., Li, Y., & Lin, Y. (2022). Late Ediacaran inertial-interchange true polar wander (IITPW) event: a new road to reconcile the enigmatic paleogeography prior to the final assembly of Gondwana. Turkish Journal of Earth Sciences: Vol. 31: No. 5, Article 1. https://doi.org/10.55730/1300-0985.1811

Wiedenbeck, M. A. P. C., Alle, P., Corfu, F. Y., Griffin, W. L., Meier, M., Oberli, F. V., ... & Spiegel, W. (1995). Three natural zircon standards for U-Th-Pb, Lu-Hf, trace element and REE analyses. Geostandards newsletter, 19(1), 1-23.

Xiao, S. H., & Narbonne, G. M. (2020). The Ediacaran Period. In Geologic time scale 2020 (pp. 521-561). Elsevier.

Youbi, N., Ernst, R.E., Söderlund, U., Boumehdi, M.A., Ait Lahna, A., Tassinari, C.C.G., El Moume, W., and Bensalah, M.K., 2020, The Central Iapetus magmatic province: An updated review and link with the ca. 580 Ma Gaskiers glaciation, in Adatte, T., Bond, D.P.G., and Keller, G., eds., Mass Extinctions, Volcanism, and Impacts: New Developments: Geological Society of America Special Paper 544, p. 35–66, https://doi.org/10.1130/2020.2544(02).